Electronic Supplementary Information

Supramolecular Glass Formation by Arene–Perfluoroarene Pairing of Three-Dimensional Macrocycles

Katsuto Onishi,[a] Shunsuke Ohtani,*[a] Kenichi Kato,[a] Shigehisa Akine,[b,c] and Tomoki Ogoshi*[a,b]

[a] *Department of Synthetic Chemistry and Biological Chemistry, Graduate School of Engineering, Kyoto University, Katsura, Nishikyo-ku, Kyoto 615-8510, Japan. E-mail: ogoshi@sbchem.kyoto-u.ac.jp*
[b] *WPI Nano Life Science Institute (WPI-NanoLSI), Kanazawa University, Kakuma-machi, Kanazawa, Ishikawa, 920-1192, Japan.*
[c] *Graduate School of Natural Science and Technology, Kanazawa University, Kakuma-machi, Kanazawa, 920-1192, Japan*

Table of Contents

General

1.1 Solution Nuclear Magnetic Resonance (NMR)

^{1}H NMR spectra were recorded at 400 MHz with a JNM-ECS400 spectrometer (JEOL RESONANCE Inc., Tokyo, Japan), ^{13}C NMR spectra were recorded at 126 MHz with a JNM-ECZ500R spectrometer (JEOL RESONANCE Inc., Tokyo, Japan) and 151 MHz with a JNM-ECZ600R spectrometer with cold probe (JEOL RESONANCE Inc., Tokyo, Japan) and ^{19}F NMR spectra were recorded at 376 MHz with a JNM-ECS400 spectrometer (JEOL RESONANCE Inc., Tokyo, Japan) and 471 MHz with a JNM-ECZ500R spectrometer (JEOL RESONANCE Inc., Tokyo, Japan). ^{1}H and ^{13}C chemical shifts were expressed as values relative to tetramethylsilane (TMS). ^{19}F chemical shifts were expressed by using the −78.8 ppm line of sodium trifluoromethanesulfonate as an external reference.

1.2 Powder X-Ray Diffraction (PXRD)

PXRD measurements were performed by a MiniFlexII (Rigaku Co., Tokyo, Japan).

1.3 Differential Scanning Calorimetry (DSC)

Results of DSC were obtained by a DSC7020 (Hitachi High-Tech Science Co., Tokyo, Japan) under a flow of dry nitrogen.

1.4 Transmittance Measurements

Transmittances of the compounds at 700 nm were recorded with a JASCO V-750 spectrophotometer. The compounds were put on a Quartz plate.

1.5 Thermogravimetry-Differential Thermal Analysis (TG-DTA) and Thermogravimetric Analysis (TGA)

Results of TG-DTA and TGA were obtained by a STA7200 (Hitachi High-Tech Science Co., Tokyo, Japan) under a flow of dry nitrogen.

1.6 Scanning Electron Microscopy (SEM) and SEM-Energy Dispersive X-ray Spectroscopy (SEM-EDX)

SEM and EDX images were acquired with HITACHI SU8220 FE-SEM+EDX.

1.7 Kubelka–Munk Transformed Diffuse Reflectance (DR) Spectroscopy

Kubelka–Munk transformed DR spectra were recorded on a JASCO V-750 spectrophotometer.

1.8 Phosphorescence Emission and Lifetime Measurements

Phosphorescence emission and phosphorescence lifetime spectra were measured on a JASCO FP-8550 spectrofluorometer.

1.9 Fourier Transform Infrared (FT-IR) Spectroscopy

Results of FT-IR spectra were recorded on a FT/IR-4X with ATR PRO 670X (JASCO Co., Tokyo, Japan).

1.10 MS Spectrometry

High Resolution Electron Ionization Fourier Transform (HR-EI-FT) mass spectra were recorded on a JEOL JMS-SX102A instrument by using the EI method in positive ion mode. High Resolution Electrospray Ionization Fourier Transform (HR-ESI-FT) mass spectra were recorded on Thermo Fisher Scientific Exactive Plus instrument and Bruker Daltonics micrOTOF II instrument by using the ESI method in positive ion mode. High Resolution Atmospheric Pressure Chemical Ionization Fourier Transform (HR-APCI-FT) mass spectra were recorded on a Thermo Fisher Scientific LTQ orbitrap XL instrument by using the APCI method in positive ion mode.

1.11 Recycling Preparative Gel Permeation Chromatography (GPC)

Recycling preparative GPC was performed with JAIGEL–2HR column and JAILaboACELC-5060.

1.12 Vapor Adsorption Measurements

Vapor adsorption isotherms were obtained by a BELSORP-max (BEL Japan Inc., Osaka, Japan) at 298 K.

1.13 Single-crystal X-ray Diffraction Analyses

Intensity data were collected on a Bruker D8 Venture diffractometer (with Cu Kα radiation, λ = 1.54178 Å). The data were corrected for Lorentz and polarization factors and for absorption by semiempirical methods based on symmetry-equivalent and repeated reflections. The structure was solved by direct methods (SHELXT) and refined by full-matrix least squares on F^2 using SHELXL 2014.[S1] Crystallographic data has been deposited with the Cambridge Crystallographic Data Centre under reference numbers CCDC 2531301 and 2531501. These data can be obtained free of charge via www.ccdc.cam.ac.uk/data_request/cif (or from the Cambridge Crystallographic Data Centre, 12 Union Road, Cambridge CB2 1EZ, UK).

Synthesis

B[6]

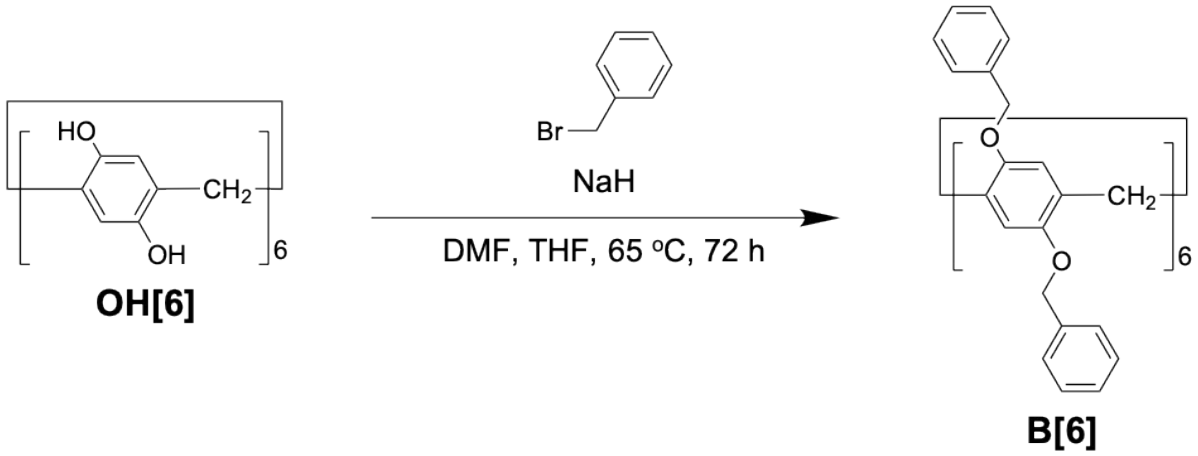

Scheme S1. Synthesis of **B[6]**.

To a flask containing pillar[6]arene with 12 hydroxyl groups[S2] (**OH[6]**; 1.56 g, 2.13 mmol) was added dry DMF (30 mL), dry THF (30 mL) and NaH (1.99 g, 80.0 mmol). The resulting mixture was stirred at 65 ℃ for 72 h under a nitrogen atmosphere whereafter benzyl bromide (8.81 g, 51.5 mmol) was added. The reaction mixture was quenched with methanol, extracted with dichloromethane, washed with brine, and then dried over anhydrous Na_2SO_4. After filtration, the solvent was evaporated under reduced pressure. The residue was purified by column chromatography (silica gel; *n*-hexane:chloroform = 1:1 to 1:2) to get a crude solid. The crude solid was then purified by preparative GPC. The obtained solid was dissolved in chloroform and the solution was poured into *n*-hexane. **B[6]** (275 mg, 0.152 mmol, yield 7.1%) was afforded as a white solid by filtration of the resulting precipitate and then vacuuming at 120 ℃ for 24 h.

^{1}H NMR (**Fig. S1**, 400 MHz, $CDCl_3$, 25 ℃) δ 7.04–7.10 (m, 60H), 6.72 (s, 12H), 4.39 (s, 24H), 3.90 (s, 12H); ^{13}C NMR (**Fig. S2**, 126 MHz, $CDCl_3$, 25 ℃) δ 150.3, 137.6, 128.2, 127.9, 127.5, 127.5, 115.3, 70.0, 31.0; HRMS (ESI) calcd. for $[C_{126}H_{108}O_{12}+Na]^+$ m/z 1835.7733, found 1835.7714.

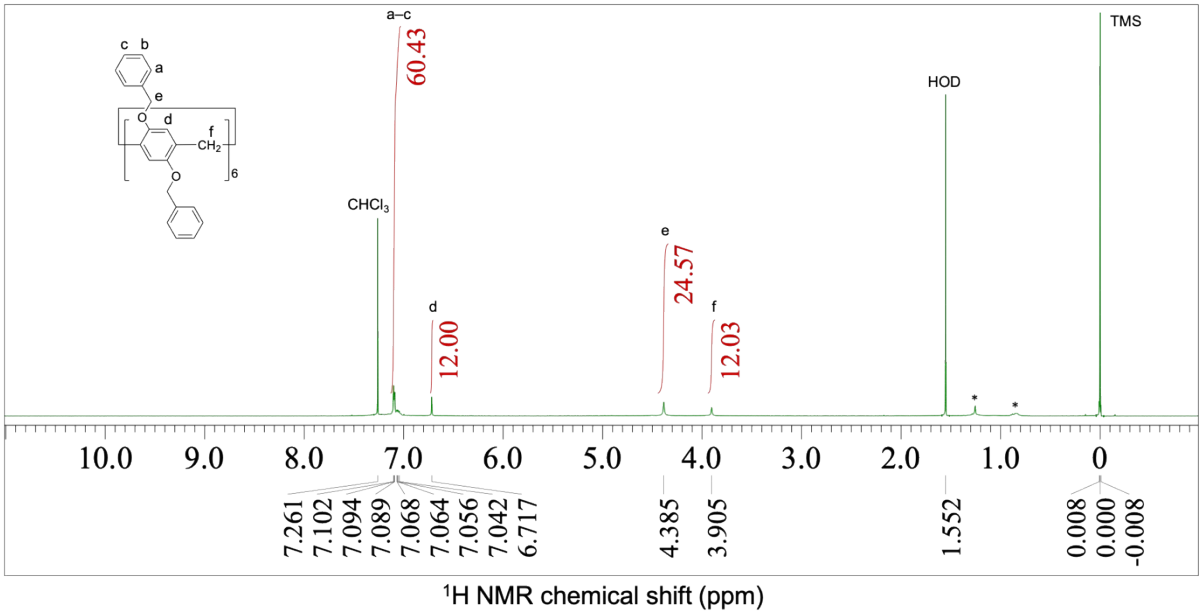

Fig. S1 ^{1}H NMR spectrum of **B[6]** ($CDCl_3$, 25 °C). The asterisk-marked signals are also observed in the spectrum of neat $CDCl_3$ and are therefore attributed to impurities present in the deuterated solvent.

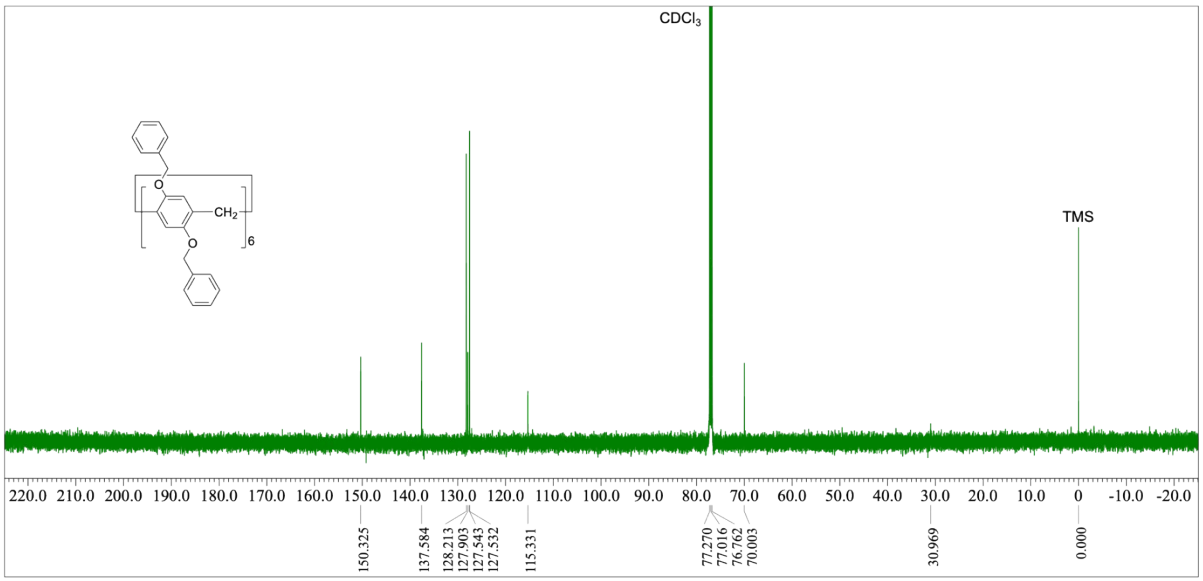

Fig. S2 ^{13}C NMR spectrum of **B[6]** ($CDCl_3$, 25 °C).

PFB[6]

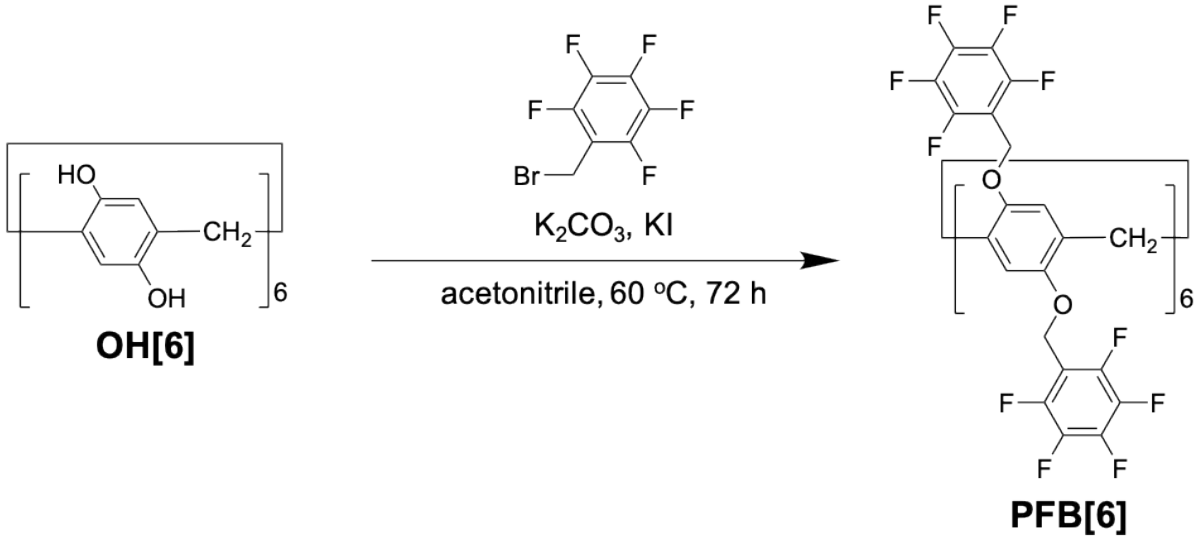

Scheme S2. Synthesis of **PFB[6]**.

To a flask containing **OH[6]** (0.582 g, 0.795 mmol) was added dry acetonitrile (60 mL), K_2CO_3 (1.65 g, 11.9 mmol) and KI (0.319 g, 1.92 mmol). The resulting mixture was stirred at 60 ℃ for 72 h under a nitrogen atmosphere whereafter 2,3,4,5,6-pentafluorobenzyl bromide (5.00 g, 19.2 mmol) was added. The reaction mixture was concentrated under reduced pressure. Water was added to the residue. The resulting mixture was extracted with dichloromethane. The organic phase was combined and washed with brine and dried over anhydrous Na_2SO_4. After filtration, the solvent was evaporated under reduced pressure. The residue was purified by column chromatography (silica gel; *n*-hexane:chloroform = 3:1) to get a crude solid. The crude solid was then purified by preparative GPC. The obtained solid was dissolved in chloroform and the solution was poured into *n*-hexane. **PFB[6]** (96.6 mg, 0.0334 mmol, yield 4.2%) was afforded as a pale-yellow solid by filtration of the resulting precipitate and then vacuuming at 120 ℃ for 24 h.

^{1}H NMR (**Fig. S3**, 400 MHz, $CDCl_3$, 25 ℃) δ 6.71 (s, 12H), 4.80 (s, 24H), 3.70 (s, 12H); ^{13}C NMR (**Fig. S4**, 151 MHz, $CDCl_3$, 25 °C) δ 150.6, 145.6, 141.6, 137.5, 128.8, 116.4, 110.5, 58.2, 29.7; ^{19}F NMR (**Fig. S5**, 376 MHz, $CDCl_3$, 25 °C) δ −143.8, −153.9, −162.7; HRMS (APCI) calcd. for $[C_{126}H_{48}O_{12}F_{60}+H]^+$ m/z 2893.2260, found 2893.2249.

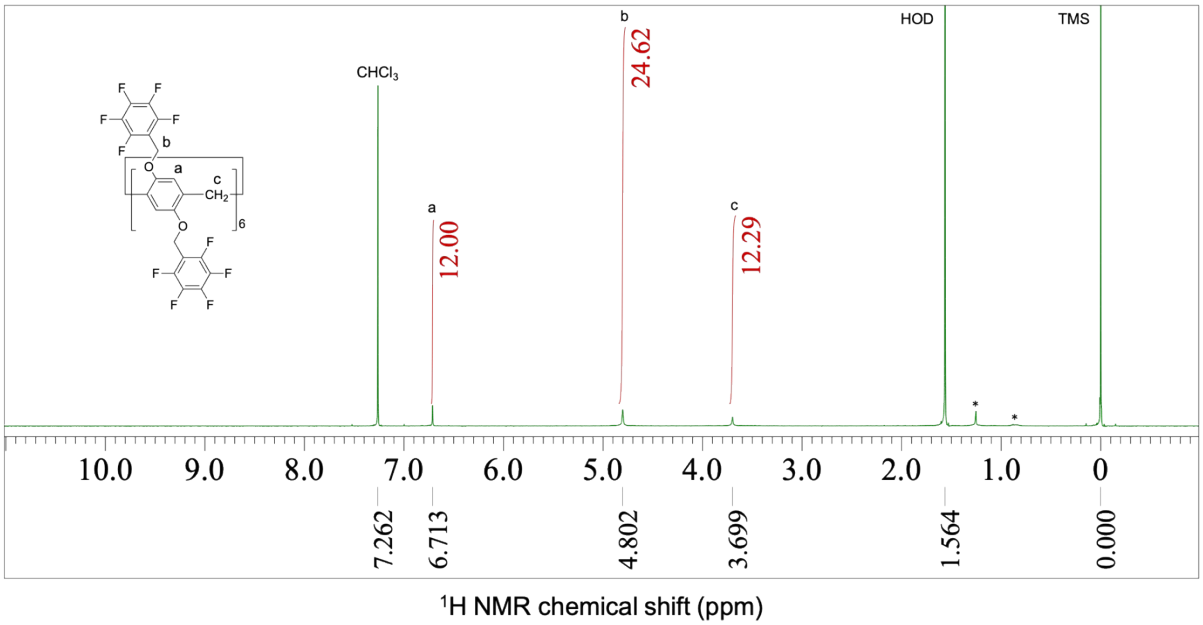

Fig. S3 ^{1}H NMR spectrum of **PFB[6]** ($CDCl_3$, 25 °C). The asterisk-marked signals are also observed in the spectrum of neat $CDCl_3$ and are therefore attributed to impurities present in the deuterated solvent.

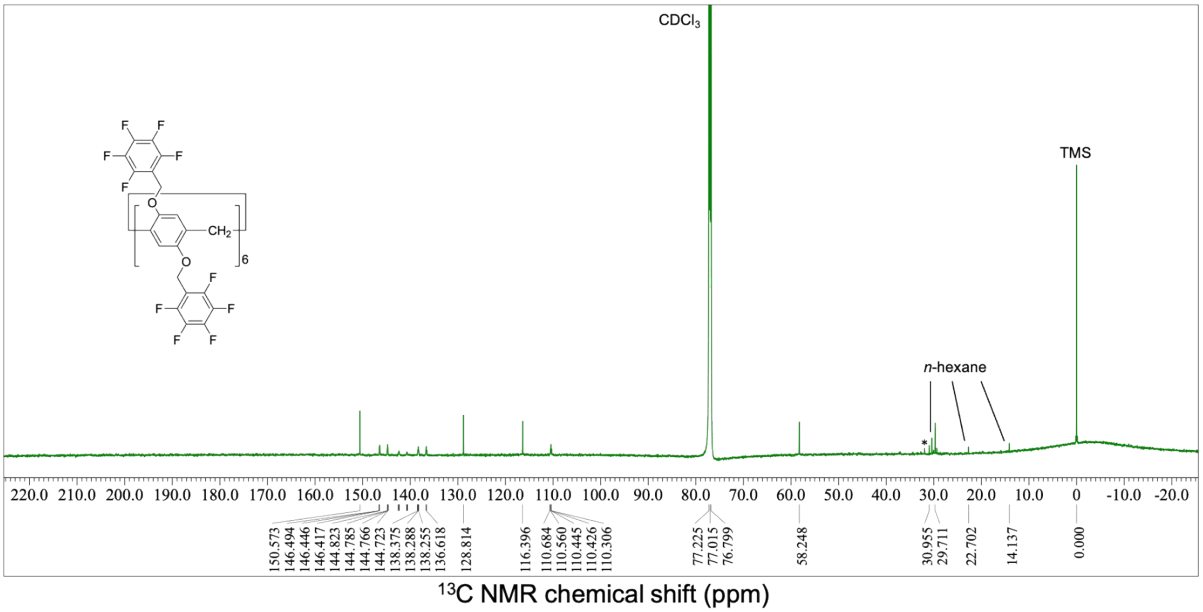

Fig. S4 ^{13}C NMR spectrum of **PFB[6]** ($CDCl_3$, 25 °C). Peaks from carbons covalently bonded with fluorine atoms were split multiply in the range of 146.6–136.5 and 110.7–110.3 ppm due to the strong ^{13}C–^{19}F coupling. Undulations in the baseline were due to use of cold probe (ECZ600) and difficult to adjust. The asterisk-marked signal is also observed in the spectrum of neat $CDCl_3$ and are therefore attributed to impurities present in the solvent. Residual *n*-hexane signals were observed despite thorough drying.

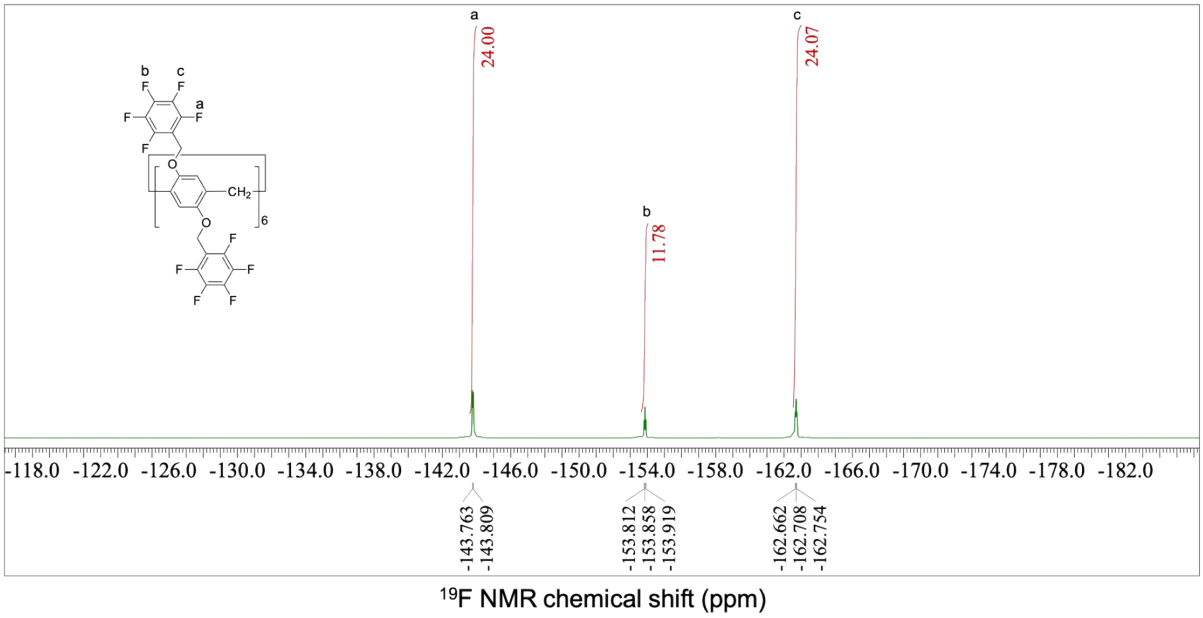

Fig. S5 ^{19}F NMR spectrum of **PFB[6]** ($CDCl_3$, 25 ℃).

PFB

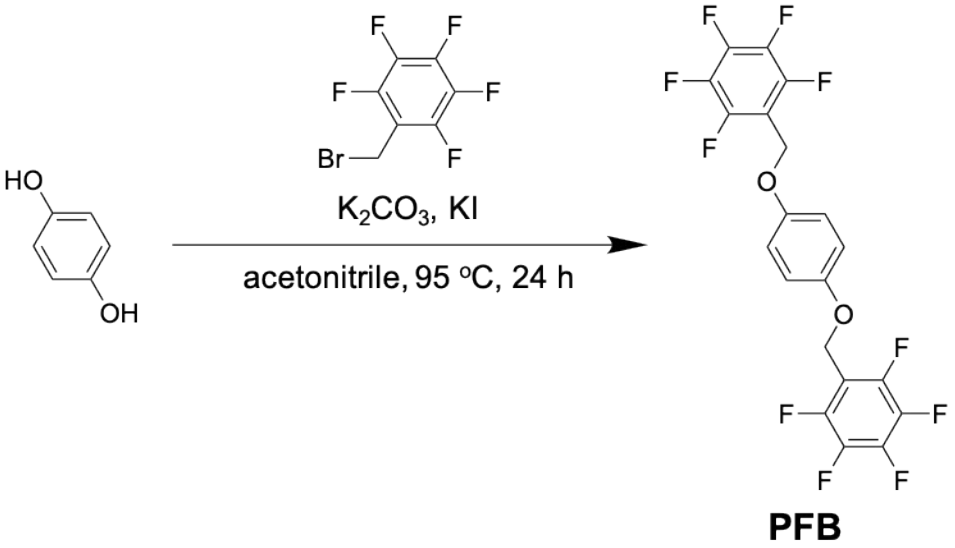

Scheme S3. Synthesis of **PFB**.

To a flask containing hydroquinone (1.05 g, 9.58 mmol) was added acetonitrile (31.9 mL), K_2CO_3 (3.97 g, 28.7 mmol) and KI (0.318 g, 1.92 mmol). The resulting mixture was stirred at 95 ℃ for 24 h whereafter 2,3,4,5,6-pentafluorobenzyl bromide (5.00 g, 19.2 mmol) was added. The solid was filtered off and, the filtrate was concentrated under reduced pressure. The residue was washed with water and dried over anhydrous Na_2SO_4. After filtration, the solvent was evaporated under reduced pressure. Column chromatography (silica gel; *n*-hexane:dichloromethane = 2:1) and then vacuuming at 120 ℃ for 24 h afforded a white solid (3.84 g, 8.17 mmol, yield 85%).

^{1}H NMR (**Fig. S6**, 400 MHz, $CDCl_3$, 25 ℃) δ 6.92 (s, 4H), 5.08 (t, $^4J_{H–F}$ = 1.5 Hz, 4H); ^{13}C NMR (**Fig. S7**, 126 MHz, $CDCl_3$, 25 ℃) δ 153.0, 145.7, 141.7, 137.6, 116.4, 110.2, 58.4; ^{19}F NMR (**Fig. S8**, 471 MHz, $CDCl_3$, 25 ℃) δ −142.9, −153.3, −162.1; HRMS (EI) calcd. for $[C_{20}H_8O_2F_{10}]^{\bullet+}$ m/z 470.0359, found 470.0364.

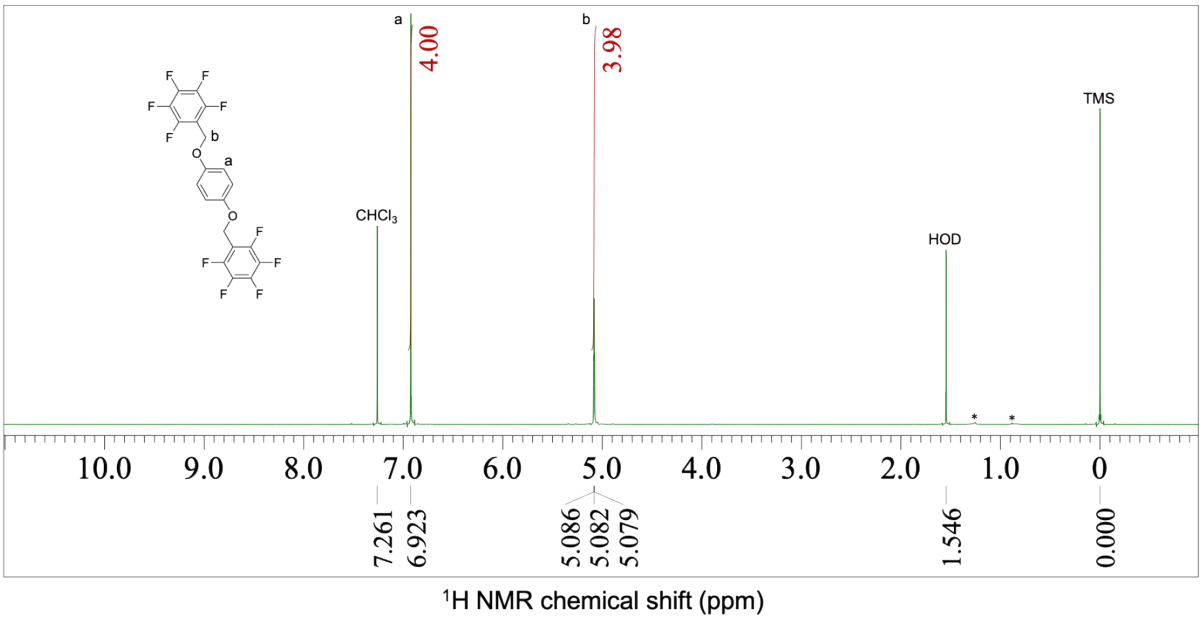

Fig. S6 ^{1}H NMR spectrum of **PFB** ($CDCl_3$, 25 °C). The asterisk-marked signals are also observed in the spectrum of neat $CDCl_3$ and are therefore attributed to impurities present in the deuterated solvent.

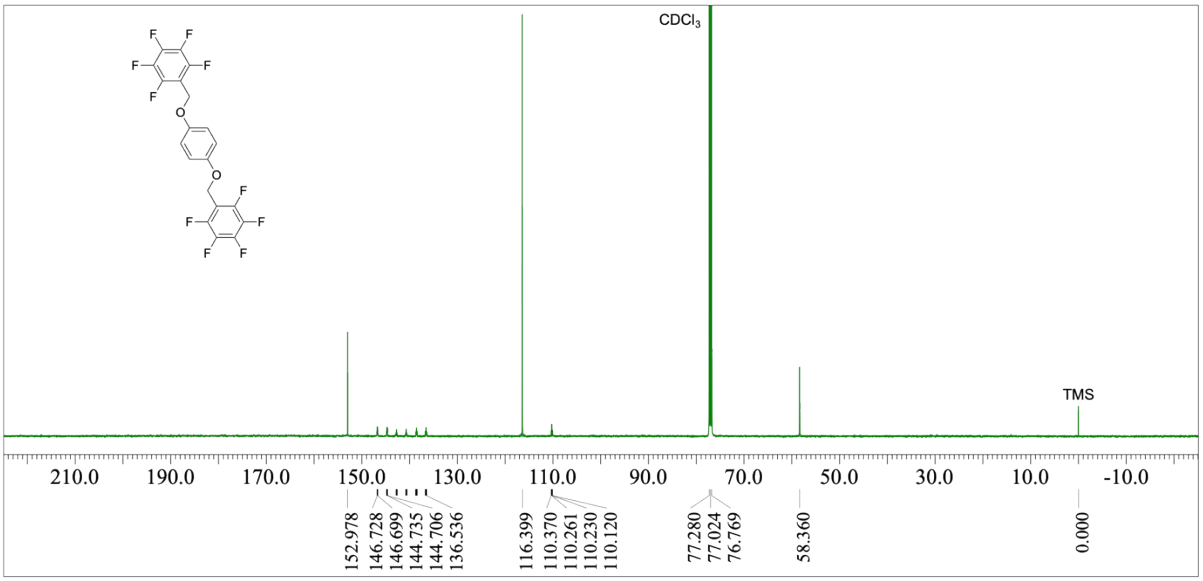

Fig. S7 ^{13}C NMR spectrum of **PFB** ($CDCl_3$, 25 °C). Peaks from carbons covalently bonded with fluorine atoms were split multiply in the range of 136.4–146.8 and 110.1–110.4 ppm due to the strong ^{13}C–^{19}F coupling.

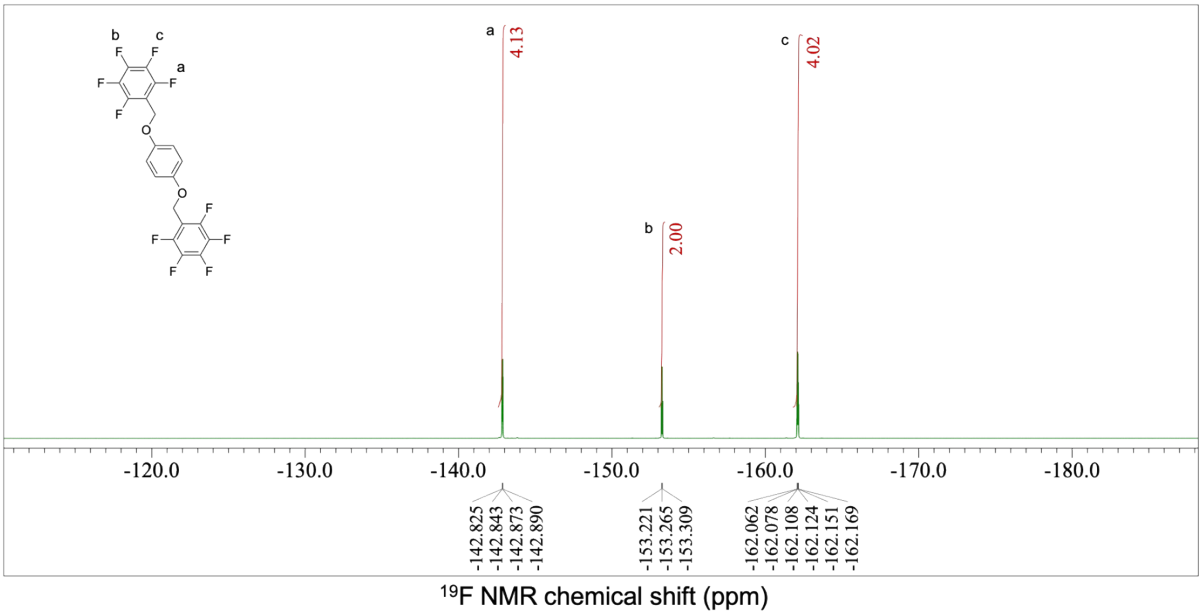

Fig. S8 ^{19}F NMR spectrum of **PFB** ($CDCl_3$, 25 °C).

PFB[5]

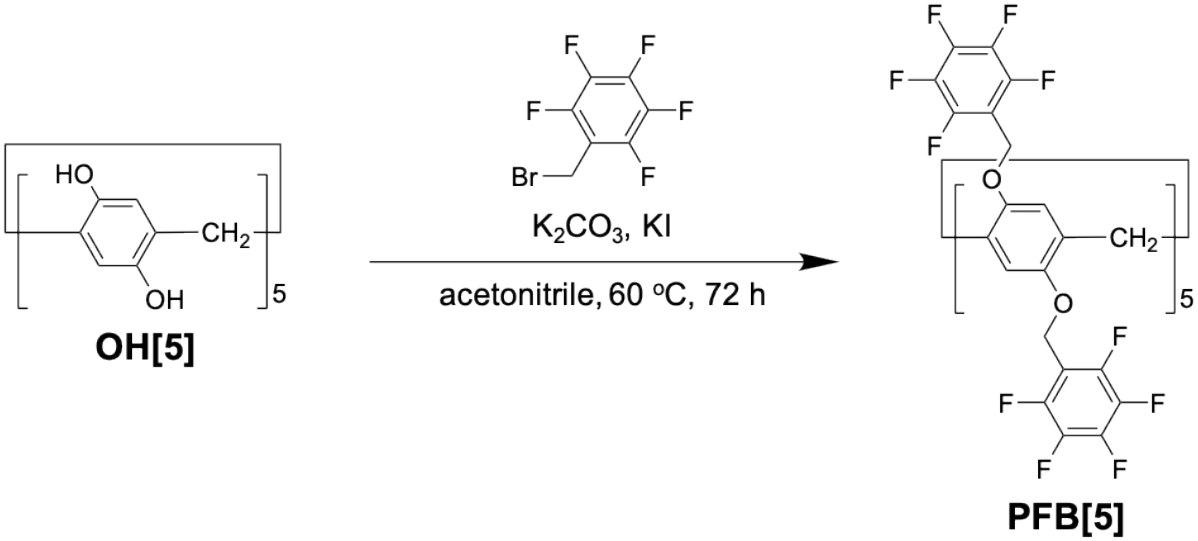

Scheme S4. Synthesis of **PFB[5]**.

To a flask containing pillar[5]arene with 10 hydroxyl groups[S3] (**OH[5]**; 0.325 g, 0.532 mmol) was added dry acetonitrile (12 mL), K_2CO_3 (1.11 g, 8.00 mmol) and KI (0.177 g, 1.07 mmol). The resulting mixture was stirred at 60 ℃ for 72 h under a nitrogen atmosphere whereafter 2,3,4,5,6-pentafluorobenzyl bromide (2.78 g, 10.7 mmol) was added. The reaction mixture was concentrated under reduced pressure. Water was added to the residue. The resulting mixture was extracted with dichloromethane. The organic phase was combined and washed with brine and dried over anhydrous Na_2SO_4. After filtration, the solvent was evaporated under reduced pressure. The residue was purified by column chromatography (silica gel; *n*-hexane:chloroform = 2:1) to get a crude solid. The crude solid was then purified by preparative GPC. The obtained solid was dissolved in chloroform and the solution was poured into *n*-hexane. **PFB[5]** (44.9 mg, 0.0186 mmol, yield 3.5%) was afforded as a pale-yellow solid by filtration of the resulting precipitate and then vacuuming at 120 ℃ for 24 h.

^{1}H NMR (**Fig. S9**, 400 MHz, $CDCl_3$, 25 ℃) δ 6.80 (s, 10H), 4.90 (dd, J = 18.1, 10.6 Hz, 20H), 3.66 (s, 10H); ^{13}C NMR (**Fig. S10**, 126 MHz, $CDCl_3$, 25 ℃) δ 150.1, 145.7, 141.6, 137.5, 129.1, 116.3, 110.7, 58.2, 29.3; ^{19}F NMR (**Fig. S11**, 376 MHz, $CDCl_3$, 25 ℃) δ −144.0, −153.8, −162.9; HRMS (APCI) calcd. for $[C_{105}H_{40}O_{10}F_{50} + H]^+$ m/z 2411.1896, found 2411.1798.

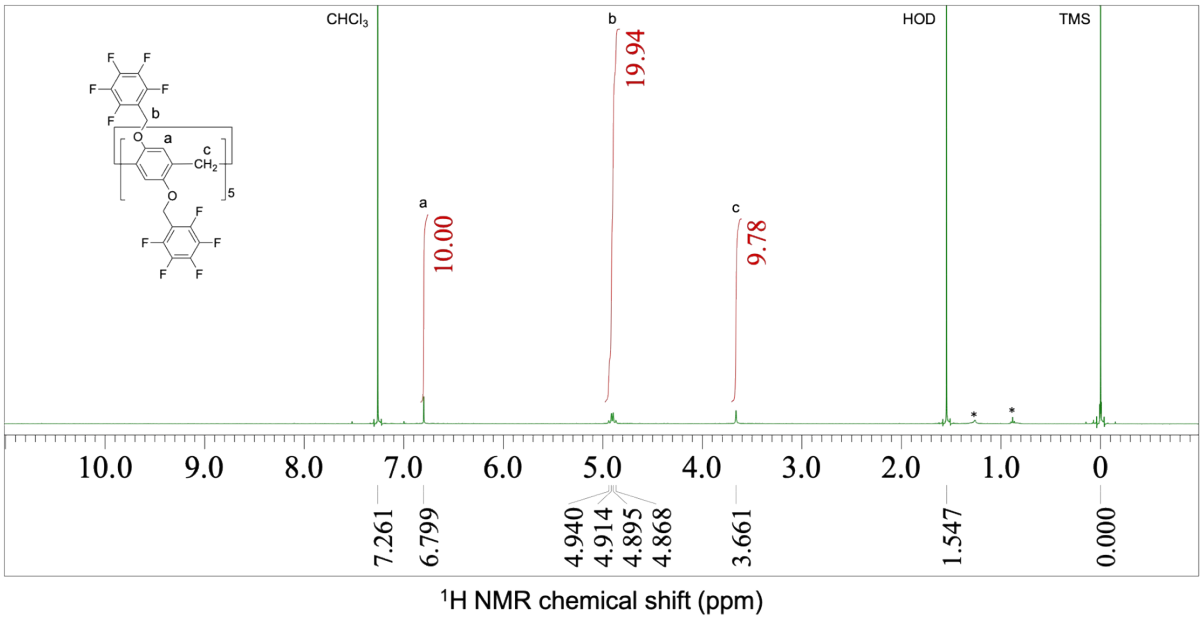

Fig. S9 ^{1}H NMR spectrum of **PFB[5]** ($CDCl_3$, 25 °C). The asterisk-marked signals are also observed in the spectrum of neat $CDCl_3$ and are therefore attributed to impurities present in the deuterated solvent.

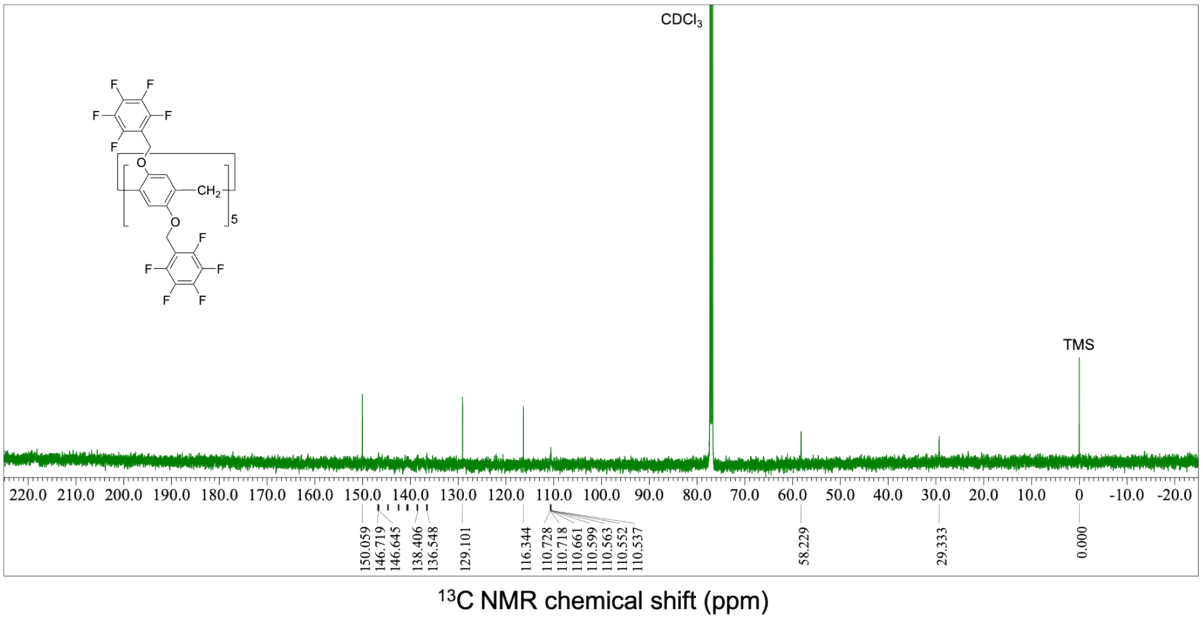

Fig. S10 ^{13}C NMR spectrum of **PFB[5]** ($CDCl_3$, 25 °C). Peaks from carbons covalently bonded with fluorine atoms were split multiply in the range of 136.4–146.8 and 110.5–110.8 ppm due to the strong ^{13}C–^{19}F coupling.

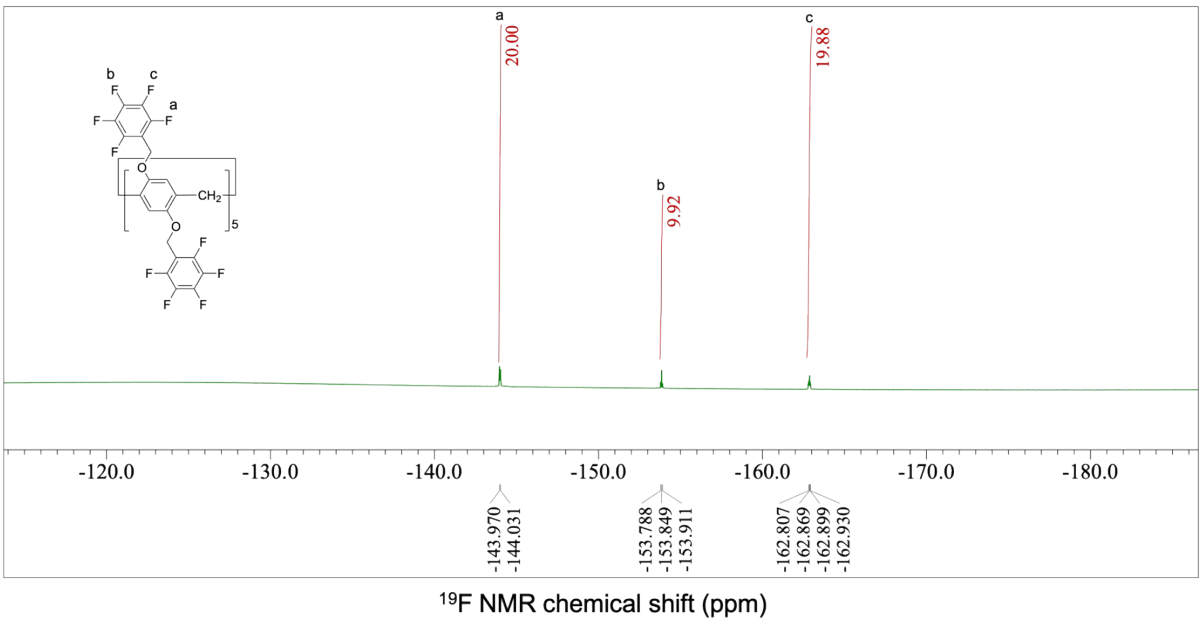

Fig. S11 ^{19}F NMR spectrum of **PFB[5]** ($CDCl_3$, 25 ℃).

E[6] and **B**

E[6][S4] (Fig. S9a), **B**[S5] (Fig. S9b) and **B[5]**[S6] (Fig. S9c) were prepared as described in the literatures.

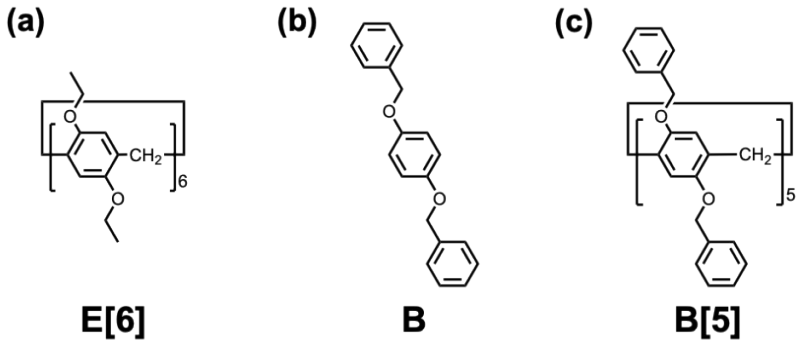

Fig. S12 Chemical structures of (a) **E[6]**, (b) **B** and (c) **B[5]**.

Preparation of ground mixture of **B[6]** and **PFB[6]**

Ground mixture of **B[6]** and **PFB[6]** was prepared by grinding **B[6]** (3.04 mg, 1.68 μmol) and **PFB[6]** (4.86 mg, 1.68 μmol) with an agate mortar.

Preparation of $\mathbf{B[6]}_1$–$\mathbf{PFB[6]}_1$

$\mathbf{B[6]}_1$–$\mathbf{PFB[6]}_1$ was prepared by heating the ground mixture of **B[6]** and **PFB[6]** at 100 °C for 10 minutes and then cooling to 25 °C.

Preparation of $\mathbf{B[6]}_1$–$\mathbf{PFB[6]}_2$

$\mathbf{B[6]}_1$–$\mathbf{PFB[6]}_2$ was prepared by grinding **B[6]** (3.04 mg, 1.68 μmol) and **PFB[6]** (9.72 mg, 3.36 μmol) with an agate mortar, heating the ground mixture at 100 °C for 10 minutes and then cooling to 25 °C.

Preparation of $\mathbf{B[6]}_2$–$\mathbf{PFB[6]}_1$

$\mathbf{B[6]}_2$–$\mathbf{PFB[6]}_1$ was prepared by grinding **B[6]** (6.08 mg, 3.36 μmol) and **PFB[6]** (4.86 mg, 1.68 μmol) with an agate mortar, heating the ground mixture at 100 °C for 10 minutes and then cooling to 25 °C.

Preparation of $\mathbf{B}_1$–$\mathbf{PFB}_1$

$\mathbf{B}_1$–$\mathbf{PFB}_1$ was prepared by grinding **B** (2.93 mg, 10.1 μmol) and **PFB** (4.74 mg, 10.1 μmol) with an agate mortar, heating the ground mixture at 150 °C for 10 minutes and then cooling to 25 °C.

Preparation of $\mathbf{B[6]}_1$–$\mathbf{PFB}_6$

$\mathbf{B[6]}_1$–$\mathbf{PFB}_6$ was prepared by grinding **B[6]** (3.04 mg, 1.68 μmol) and **PFB** (4.74 mg, 10.1 μmol) with an agate mortar, heating the ground mixture at 130 °C for 10 minutes and then cooling to 25 °C.

Preparation of $\mathbf{PFB[6]}_1$–$\mathbf{B}_6$

$\mathbf{PFB[6]}_1$–$\mathbf{B}_6$ was prepared by grinding **PFB[6]** (4.86 mg, 1.68 μmol) and **B** (2.93 mg, 10.1 μmol) with an agate mortar, heating the ground mixture at 130 °C for 10 minutes and then cooling to 25 °C.

Preparation of $\mathbf{B[6]}_1$–$\mathbf{E[6]}_1$

$\mathbf{B[6]}_1$–$\mathbf{E[6]}_1$ was prepared by grinding **B[6]** (4.56 mg, 2.52 μmol) and **E[6]** (2.69 mg, 2.52 μmol) with an agate mortar, heating the ground mixture at 180 °C for 10 minutes and then cooling to 25 °C.

Preparation of $\mathbf{PFB[6]}_1$–$\mathbf{E[6]}_1$

$\mathbf{PFB[6]}_1$–$\mathbf{E[6]}_1$ was prepared by grinding **PFB[6]** (4.86 mg, 1.68 μmol) and **E[6]** (1.80 mg, 1.68 μmol) with an agate mortar, heating the ground mixture at 180 °C for 10 minutes and then cooling to 25 °C.

Preparation of $\mathbf{B[5]}_1$–$\mathbf{PFB[5]}_1$

$\mathbf{B[5]}_1$–$\mathbf{PFB[5]}_1$ was prepared by grinding **B[5]** (2.54 mg, 1.68 μmol) and **PFB[5]** (4.06 mg, 1.68 μmol) with an agate mortar, heating the ground mixture at 180 °C for 10 minutes and then cooling to 25 °C.

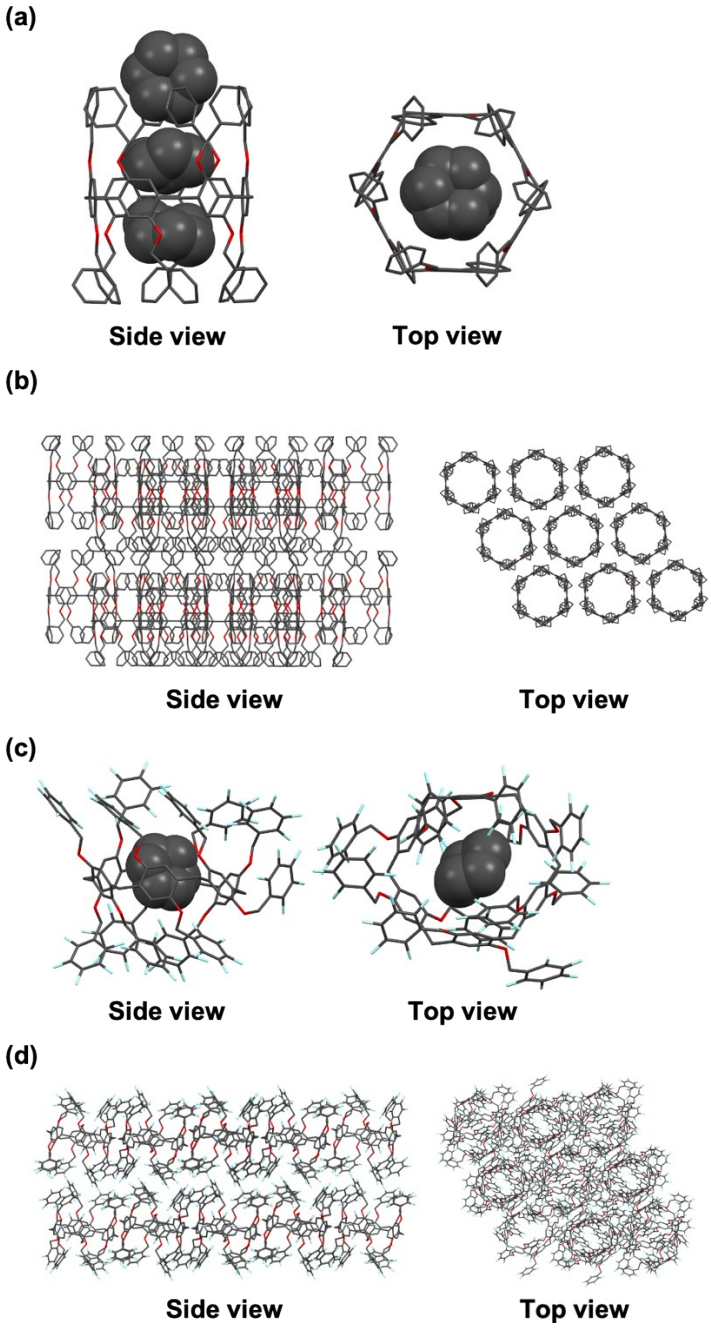

Fig. S13 (a) Single-crystal structures and (b) the packing structures of complex of **B[6]** with cyclohexane. (c) Single-crystal structures and (d) the packing structures of complex of **PFB[6]** with cyclohexane. In the structures, C: gray, O: red, F: light blue; all H atoms and cyclohexane guest molecules in (b) and (d) are omitted for clarity.

Single crystals **B[6]** of and **PFB[6]** were obtained by vapor diffusion of cyclohexane into dichloromethane solutions. Single-crystal X-ray diffraction (SCXRD) analyses revealed that the two crystal structures were different each other. **B[6]** formed a 1:3 host–guest complex with cyclohexane. The complex formed a highly symmetrical pillar-shaped structure, resulting in the formation of one-dimensional channel assemblies. In contrast, **PFB[6]** formed a complex with cyclohexane in a 1:1 ratio. The orientations of six dipentafluorobenzyloxybenzene units are not aligned and assembled to slipped-stacked structure.

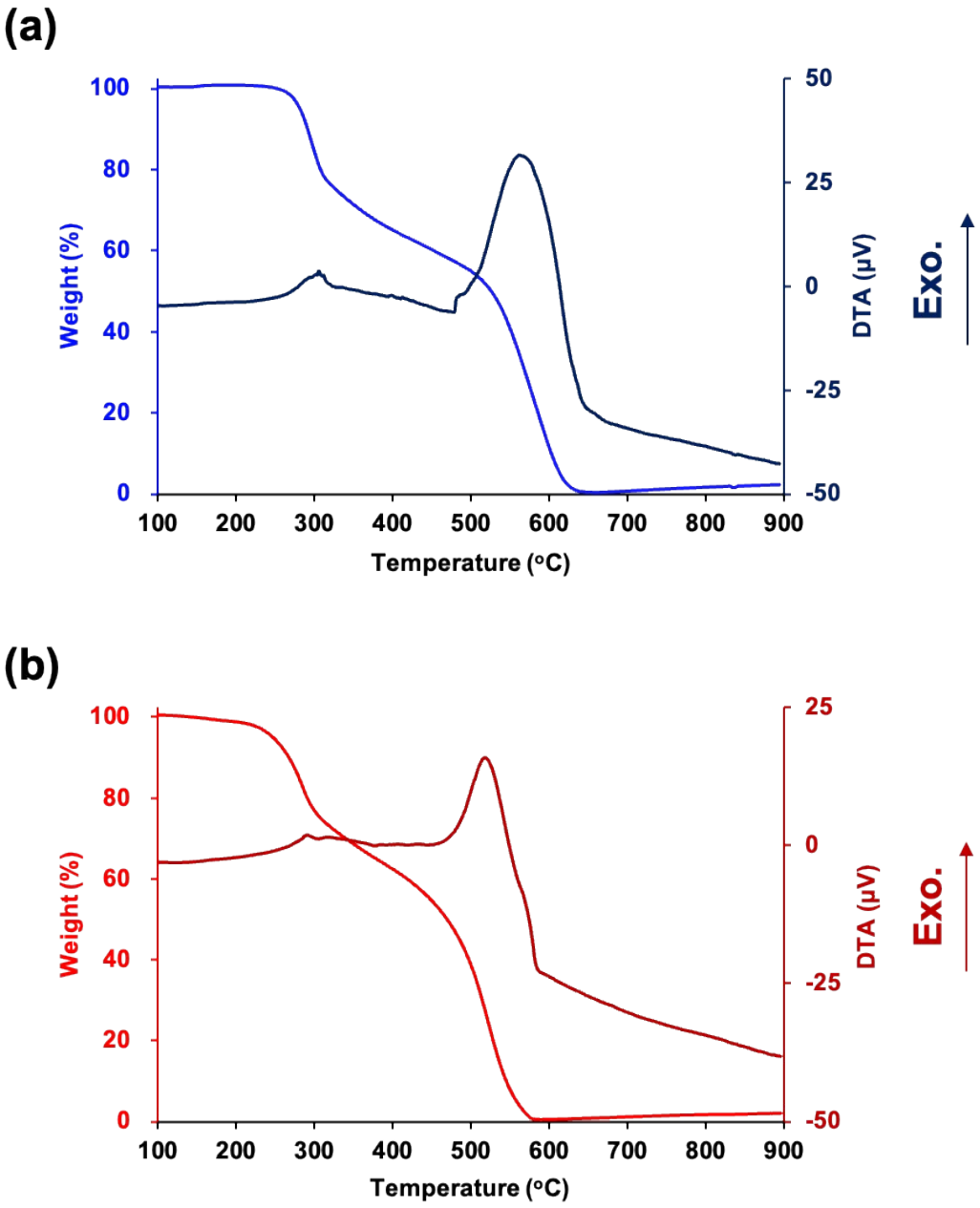

Fig. S14 TG-DTA traces of (a) **B[6]** and (b) **PFB[6]** (scanning rate: 10 °C/min).

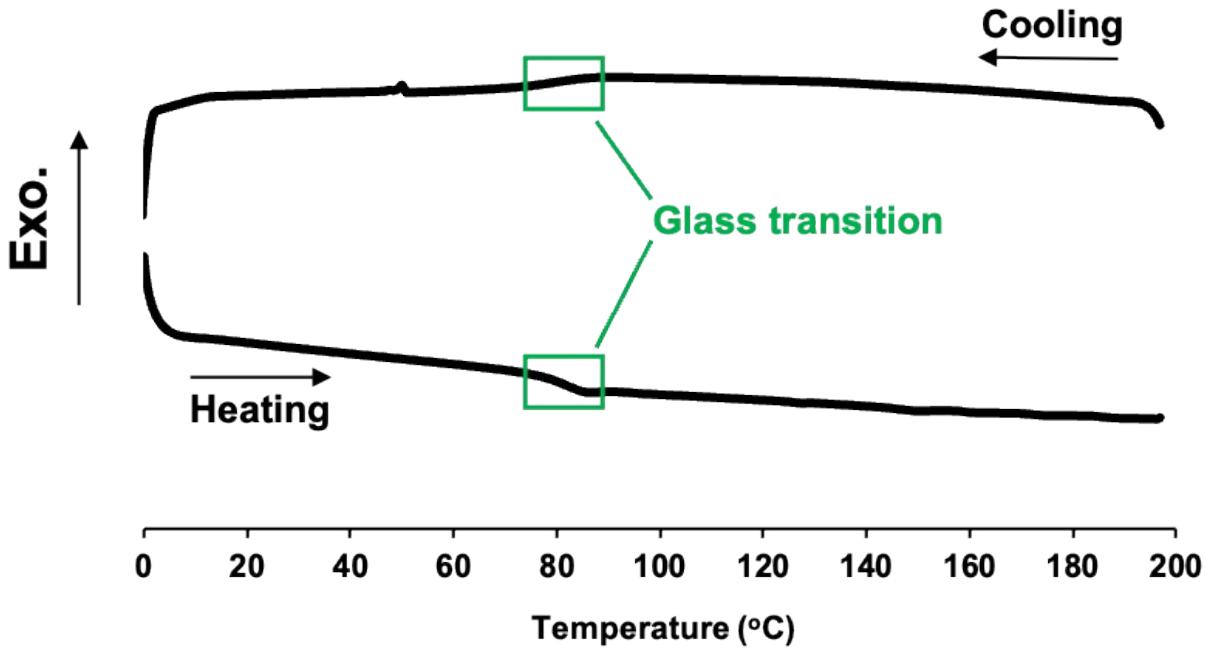

Fig. S15 DSC second heating and cooling curves of the ground mixture of **B[6]** and **PFB[6]** (scanning rate: 10 °C/min).

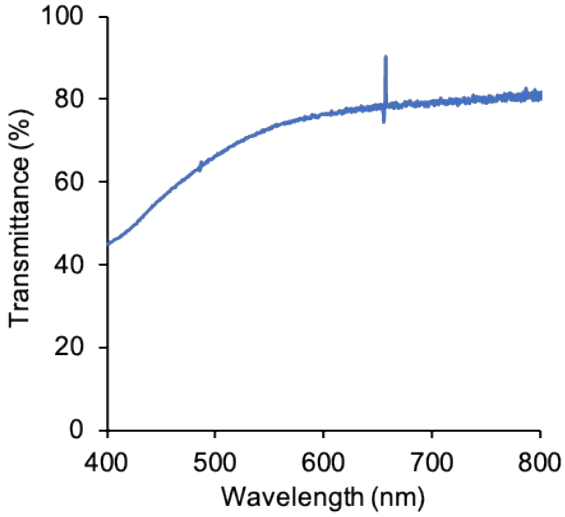

Fig. S16 Transmittance curve of **B[6]**$_1$–**PFB[6]**$_1$.

Supporting Note 1

To examine the porosity of **B[6]**$_1$–**PFB[6]**$_1$, adsorption measurements were performed. Cyclohexane vapor was used as the adsorbate because it can be taken up into the cavities of pillar[6]arenes.[S7–S9] Adsorption isotherms of cyclohexane vapor revealed that **B[6]**$_1$–**PFB[6]**$_1$ exhibited almost no adsorption, whereas **B[6]** and **PFB[6]** showed adsorption in the high-pressure region (Fig. S17). These results suggest the loss of the pore structure of **B[6]**$_1$–**PFB[6]**$_1$ to such an extent that the adsorption of cyclohexane vapor no longer occurred.

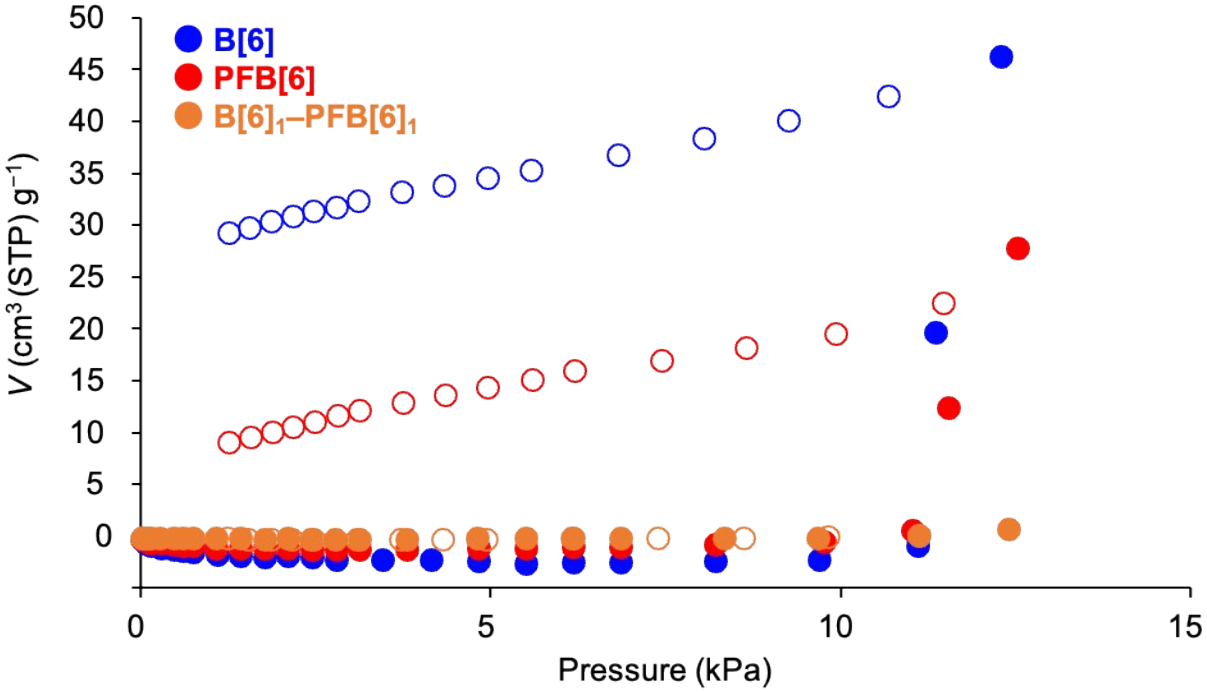

Fig. S17 Adsorption and desorption isotherms of cyclohexane for **B[6]** (blue), **PFB[6]** (red) and **B[6]**$_1$–**PFB[6]**$_1$ (orange). Solid and open circles represent adsorption and desorption, respectively.

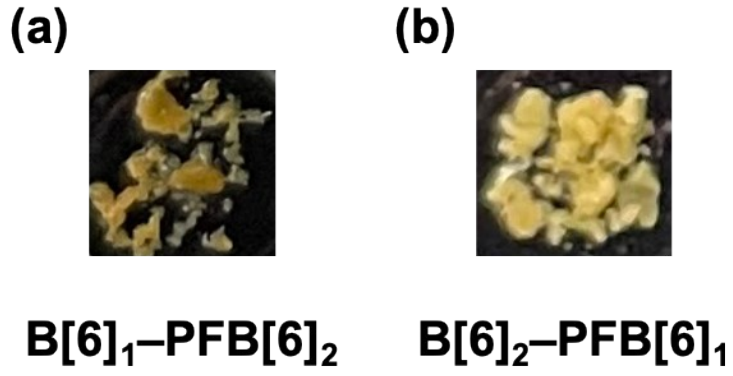

Fig. S18 Photographs of (a) **B[6]**$_1$–**PFB[6]**$_2$ and (b) **B[6]**$_2$–**PFB[6]**$_1$.

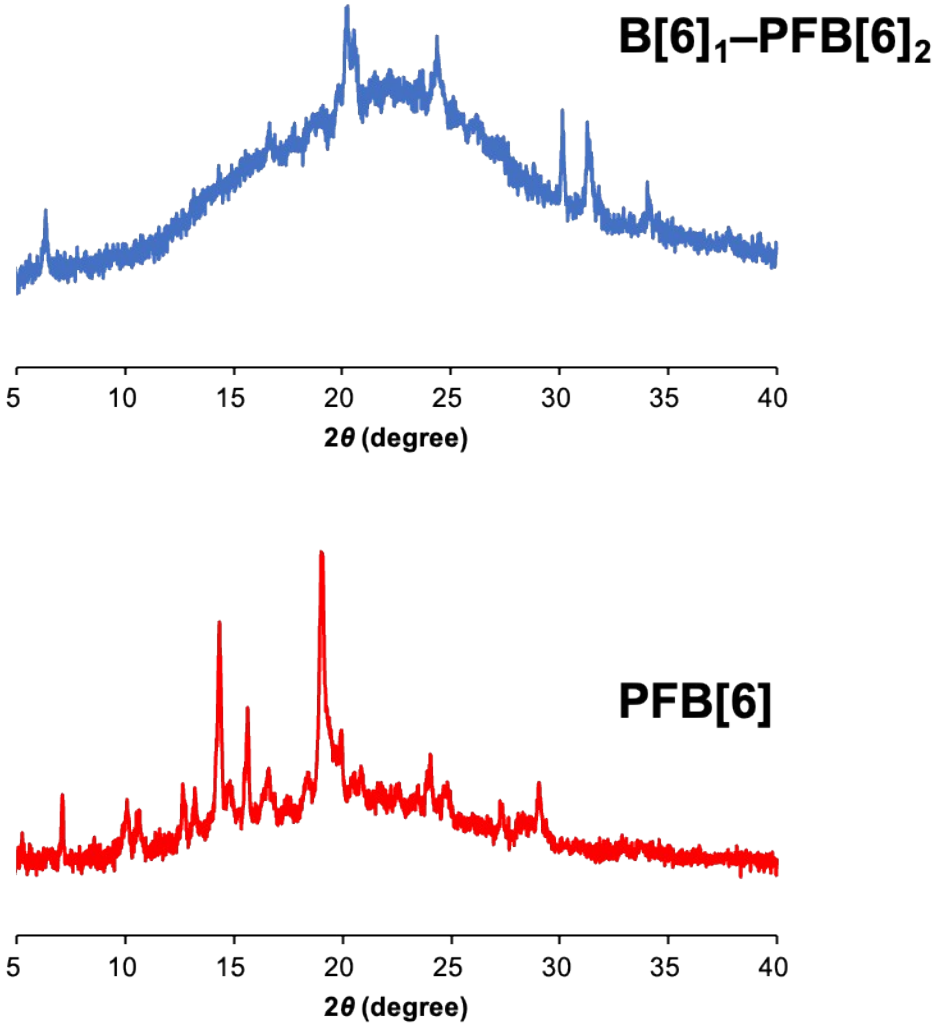

Fig. S19 PXRD patterns of **B[6]**$_1$–**PFB[6]**$_2$ (upper side) and **PFB[6]** (lower side).

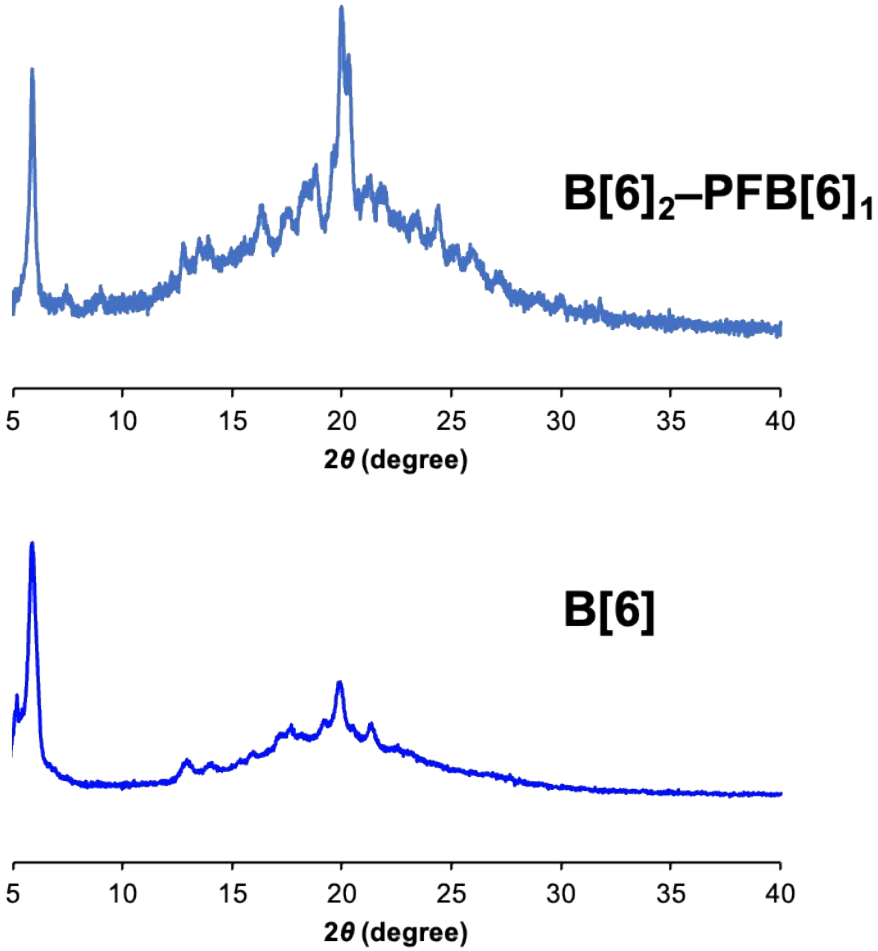

Fig. S20 PXRD patterns of **B[6]**$_2$–**PFB[6]**$_1$ (upper side) and **B[6]** (lower side).

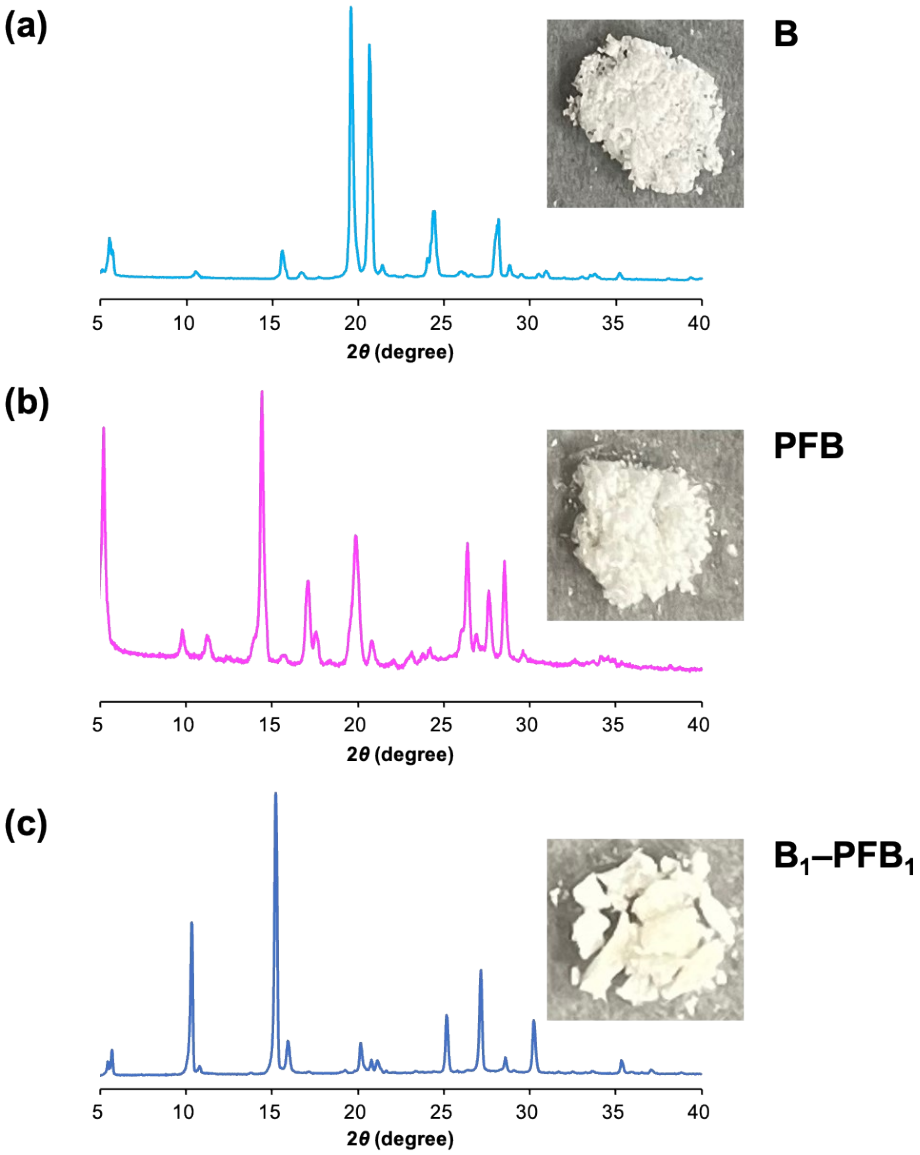

Fig. S21 PXRD patterns and photographs of (a) **B**, (b) **PFB** and (c) $\mathbf{B}_1$–$\mathbf{PFB}_1$.

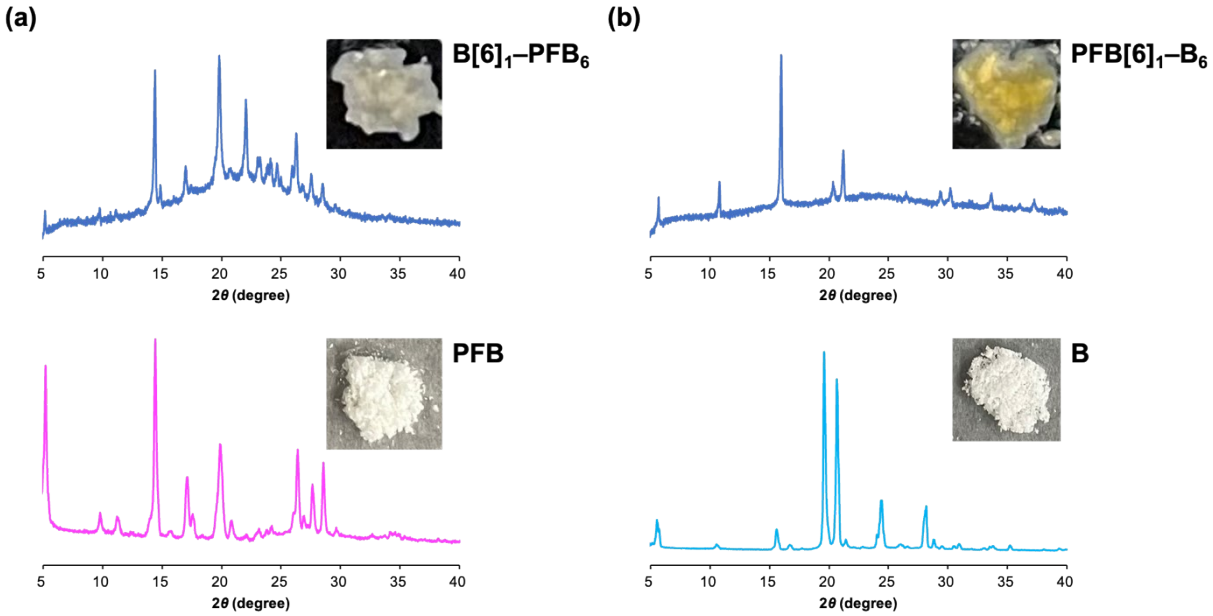

Fig. S22 PXRD patterns and photographs of (a) **B[6]**$_1$–**PFB**$_6$ (upper side) and **PFB** (lower side) and (b) **PFB[6]**$_1$–**B**$_6$ (upper side) and **B** (lower side).

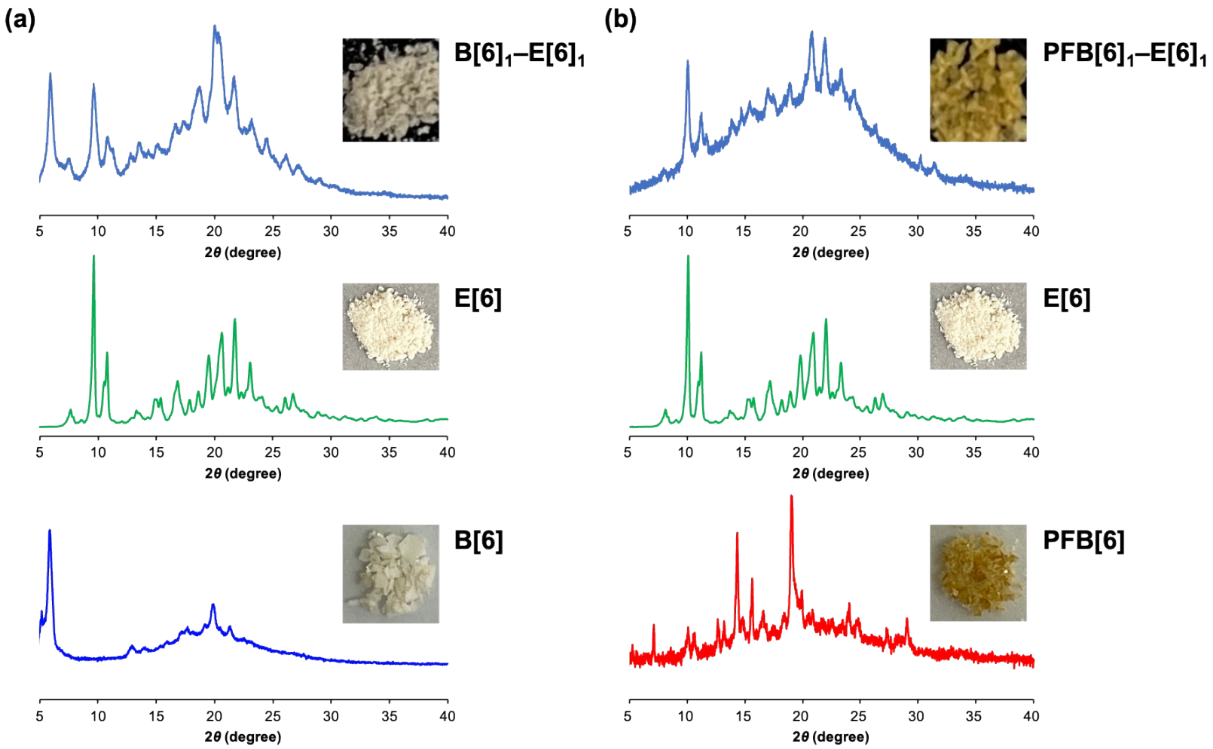

Fig. S23 PXRD patterns and photographs of (a) **B[6]**$_1$–**E[6]**$_1$ (top), **E[6]** (middle) and **B[6]** (bottom) and (b) **PFB[6]**$_1$–**E[6]**$_1$ (top), **E[6]** (middle) and **PFB[6]** (bottom).

Supporting Note 2

To further confirm the necessity of the pillar[6]arene scaffold for the glass formation, pillar[5]arene derivatives bearing benzyl groups (**B[5]**; Fig. S12c) and pentafluorobenzyl groups (**PFB[5]**; Scheme S4 and Figs. S9–S11) were also synthesized. DSC curves revealed that **B[5]** and **PFB[5]** exhibit melting points at 177 and 151 °C, respectively (Fig. S24). The observed melting behavior of **B[5]** and **PFB[5]**, in contrast to the absence of melting transitions in **B[6]** and **PFB[6]**, could be attributed to their smaller number of repeating units and less efficient molecular packing arising from their pentagonal, lower-symmetry structures, resulting in weakened intermolecular interactions and reduced thermal stability of the crystals. Moreover, the mixture of these two pillar[5]arene derivatives (**B[5]**$_1$–**PFB[5]**$_1$) was a powder, and its PXRD pattern was a superposition of those of the parent compounds (Fig. S25), indicating that no glass formation occurred. These results suggest that the smaller pillar[5]arene scaffold more readily undergoes ordered packing and crystallization, and that the arene–perfluoroarene interaction is insufficient to generate a mixed amorphous phase in this case. By contrast, the bulkier pillar[6]arene scaffold appears to increase packing frustration in the mixed state, thereby enabling supramolecular glass formation from two crystalline components without melt-processing.

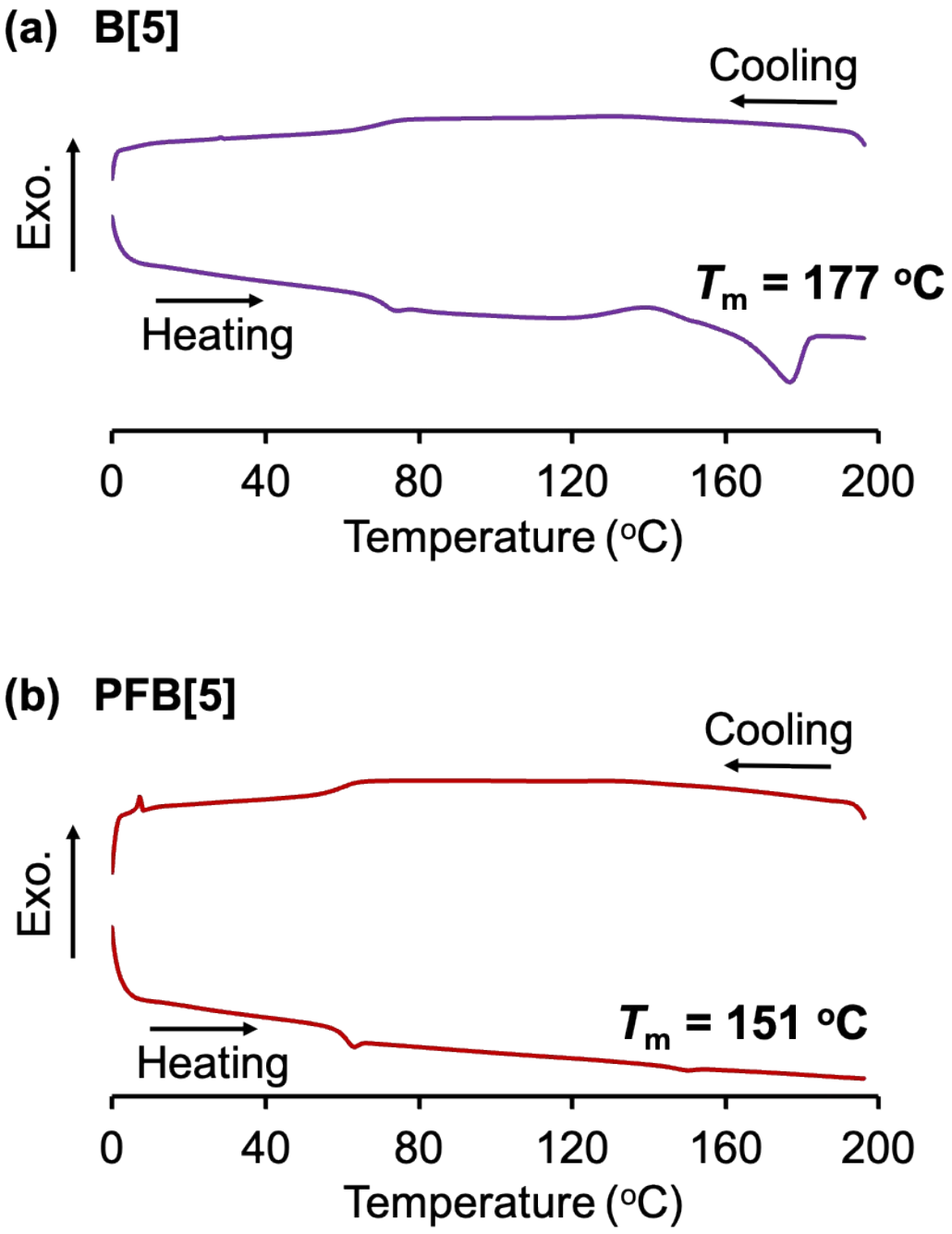

Fig. S24 DSC second heating and cooling curves of (a) **B[5]** and (b) **PFB[5]** (scanning rates: 10 °C/min). Upon heating above each endothermic peak temperature, melting of the compounds was visually confirmed.

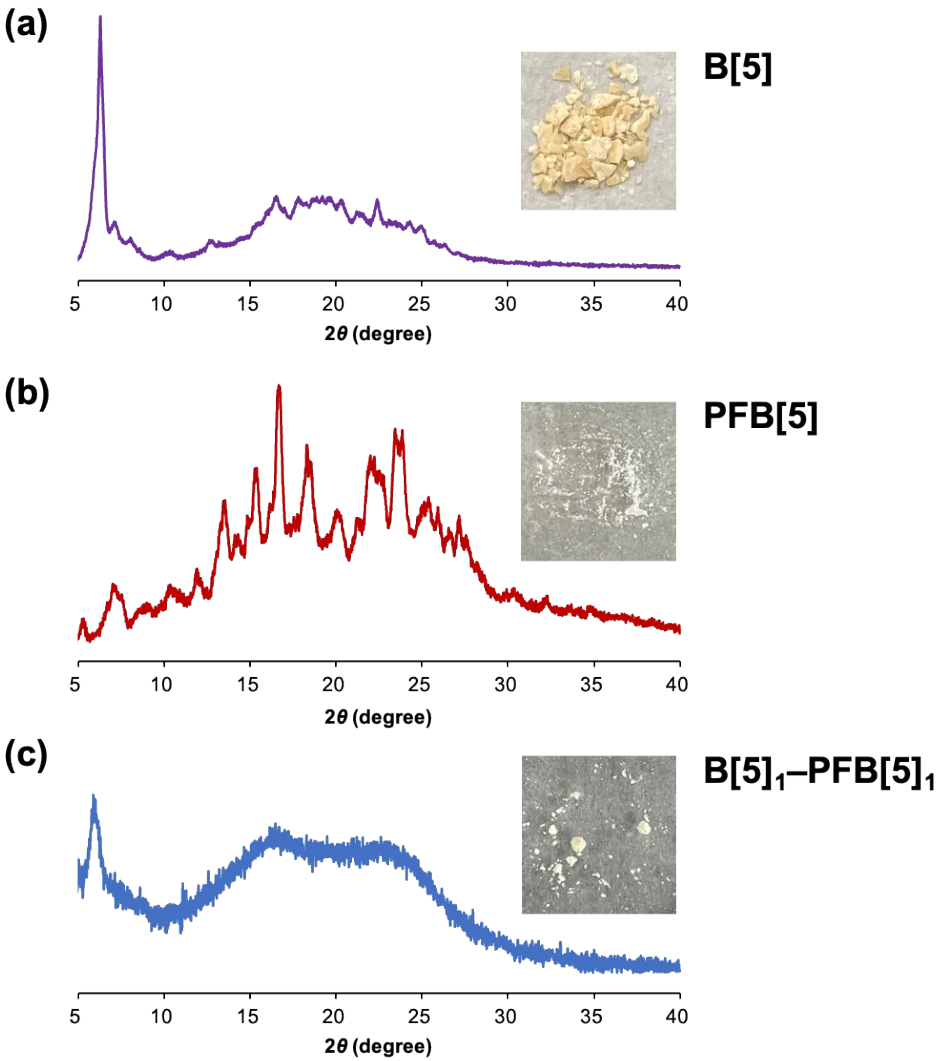

Fig. S25 PXRD patterns and photographs of (a) **B[5]**, (b) **PFB[5]** and (c) **B[5]**$_1$–**PFB[5]**$_1$.

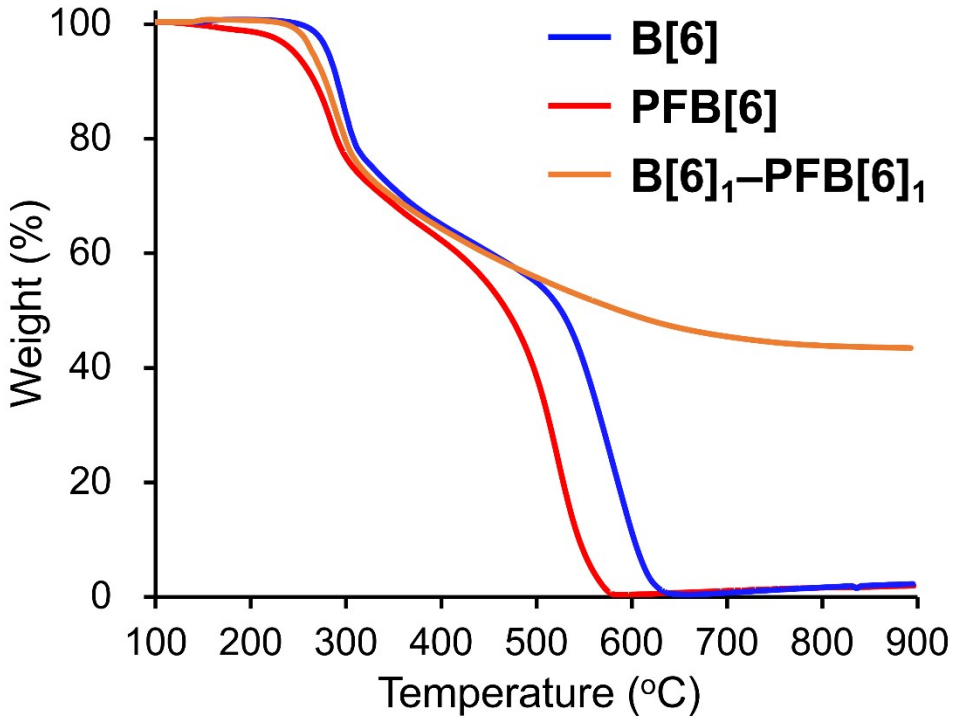

Fig. S26 TG curves of **B[6]**, **PFB[6]** and **B[6]**$_1$–**PFB[6]**$_1$ (scanning rate: 10 °C/min).

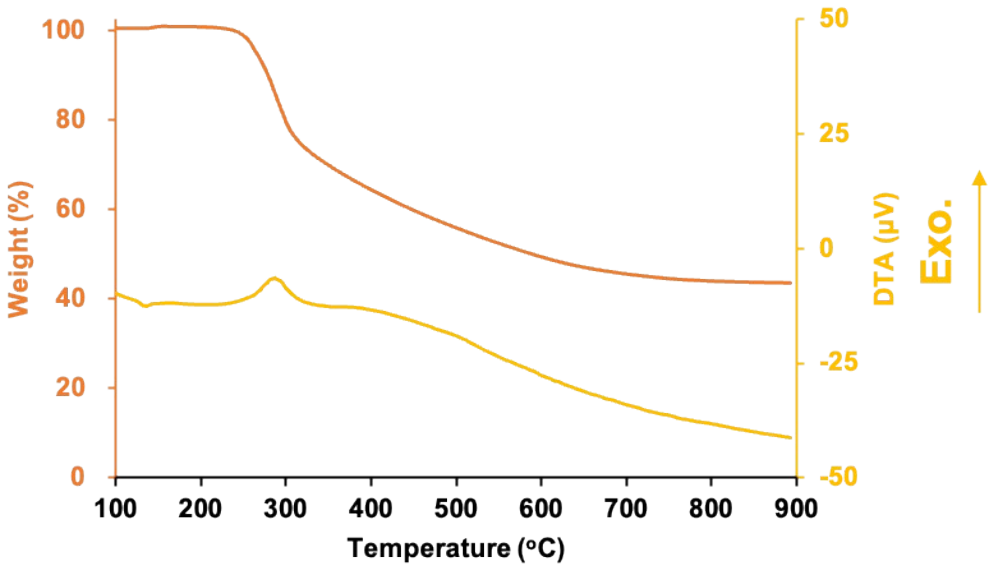

Fig. S27 TG-DTA trace of **B[6]**$_1$–**PFB[6]**$_1$ (scanning rate: 10 °C/min).

An exothermic peak was observed in the DTA curve between approximately 270 and 310 °C. This thermal event suggests that cross-linking reactions may occur in this temperature range between the benzyl moieties of **B[6]** and the pentafluorobenzyl moieties of **PFB[6]**. As a consequence of this cross-linking process, **B[6]**$_1$–**PFB[6]**$_1$ is expected to yield a carbonaceous residue even upon heating to 900 °C.[S10]

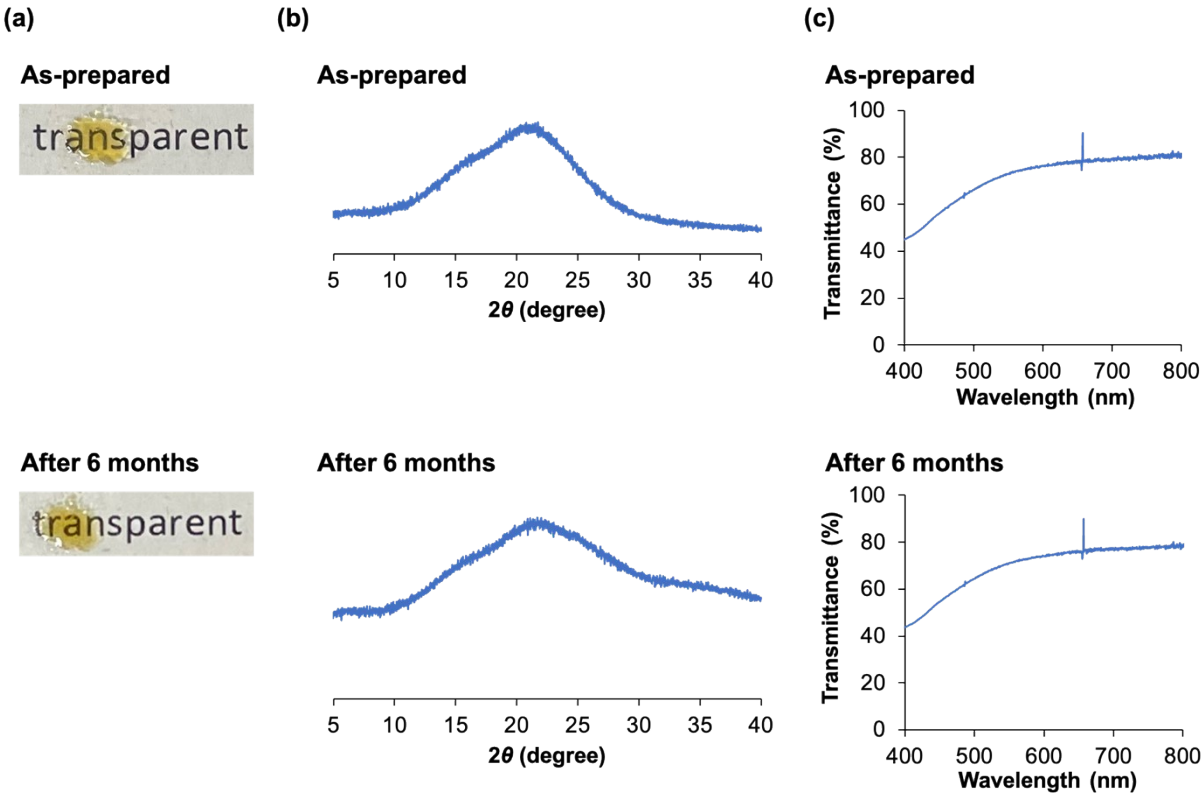

Fig. S28 (a) Photographs, (b) PXRD patterns and (c) transmittance curves of **B[6]**$_1$–**PFB[6]**$_1$: as-prepared (upper sides) and after storing for 6 months under an air atmosphere at room temperature (lower sides).

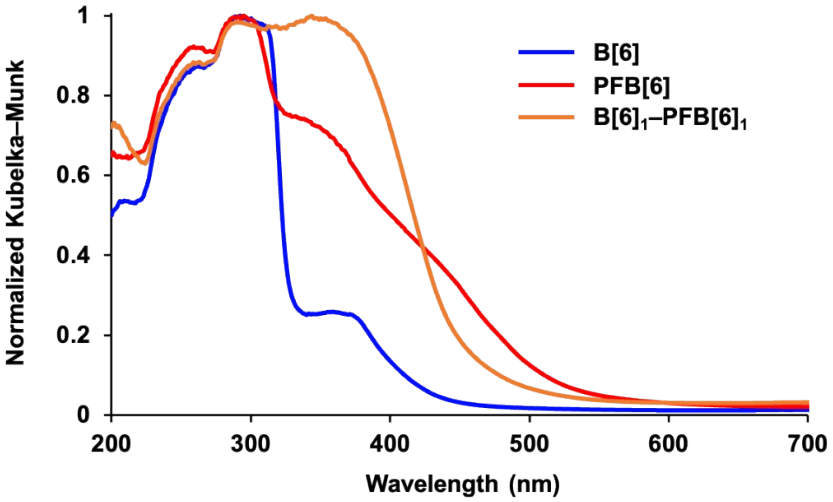

Fig. S29 Kubelka–Munk transformed DR spectra of **B[6]**, **PFB[6]** and **B[6]**$_1$–**PFB[6]**$_1$. All spectra were recorded at room temperature in air.

Supporting Note 3

To further investigate the RTP mechanism of **B[6]**$_1$–**PFB[6]**$_1$, phosphorescence measurements were conducted under controlled atmospheres (Fig. S30 and S31). The apparatus for measurement under sealed atmospheres often requires approximately 100 mg of sample; however, only approximately 10 mg of **B[6]**$_1$–**PFB[6]**$_1$ could be prepared because of the low yields of **B[6]** and **PFB[6]**. Consequently, although the phosphorescence intensity and lifetime could be measured accurately, the signal intensity was insufficient, resulting in spectra with a low signal-to-noise ratio and negative intensity artifacts in the long-wavelength region of the emission spectra. At room temperature, the emission intensity showed little difference between under air and nitrogen, whereas it decreased by approximately half under oxygen without complete quenching (Fig. S30a). The partial quenching by oxygen suggests that the RTP of **B[6]**$_1$–**PFB[6]**$_1$ originates from a triplet excited state. In addition, the phosphorescence lifetimes were nearly identical under all atmospheres (Fig. S30b). These results suggest that the dense arene–perfluoroarene stacking in the **B[6]**$_1$–**PFB[6]**$_1$ glass have already restricted the diffusion and penetration of oxygen molecules, thereby suppressing oxygen-induced quenching. Consequently, the phosphorescence intensity and lifetime are largely insensitive to the surrounding atmosphere. Furthermore, at 77 K, the emission peaks near the maximum became sharper and a new shoulder emerged at approximately 440–510 nm (Fig. S31a), compared with the single broad peak observed at room temperature (Fig. 5a). This behavior might be caused by suppression of thermal fluctuations at low temperature, allowing resolution of the vibronic structure and partial separation of vibronic components. Moreover, the phosphorescence lifetime increased from 70 ms at room temperature (Fig. 5b) to 159 ms at 77 K (Fig. S31b). This enhancement could be attributed to suppression of nonradiative decay pathways under low-temperature conditions due to the reduced molecular motions and vibrational relaxation.

To exclude the possibility that the observed RTP of **B[6]**$_1$–**PFB[6]**$_1$ may originate from trace impurities, the high purity of the samples was confirmed by NMR spectroscopy (Fig. S1 and S2 for **B[6]** and Fig. S3–S5 for **PFB[6]**). In addition, a previous report demonstrated that a crystalline pillar[5]arene derivative bearing methoxy groups exhibits phosphorescence at 77 K,[S11] indicating that the pillar[*n*]arene scaffold itself has the potential to support phosphorescence under sufficiently rigid conditions at low temperature. Moreover, the co-crystal of the unit models **B**$_1$–**PFB**$_1$ exhibits phosphorescence at room temperature (Fig. S33), suggesting that arene–perfluoroarene interactions can contribute to RTP. Taken together, these results support the conclusion that the RTP of **B[6]**$_1$–**PFB[6]**$_1$ originates from the molecular glass itself rather than from trace impurities or external factors.

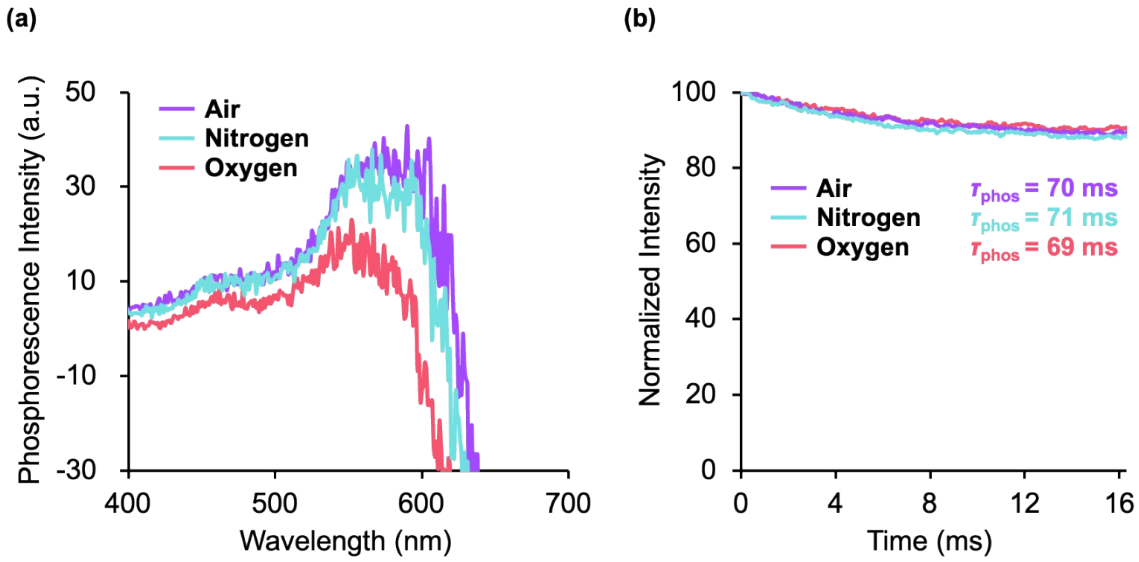

Fig. S30 (a) Steady-state phosphorescence spectra (λ_{ex} = 344 nm) and (b) RTP lifetime decay curves (λ_{ex} = 344 nm and λ_{det} = 562 nm) of **B[6]**$_1$–**PFB[6]**$_1$ recorded at room temperature under air, nitrogen and oxygen.

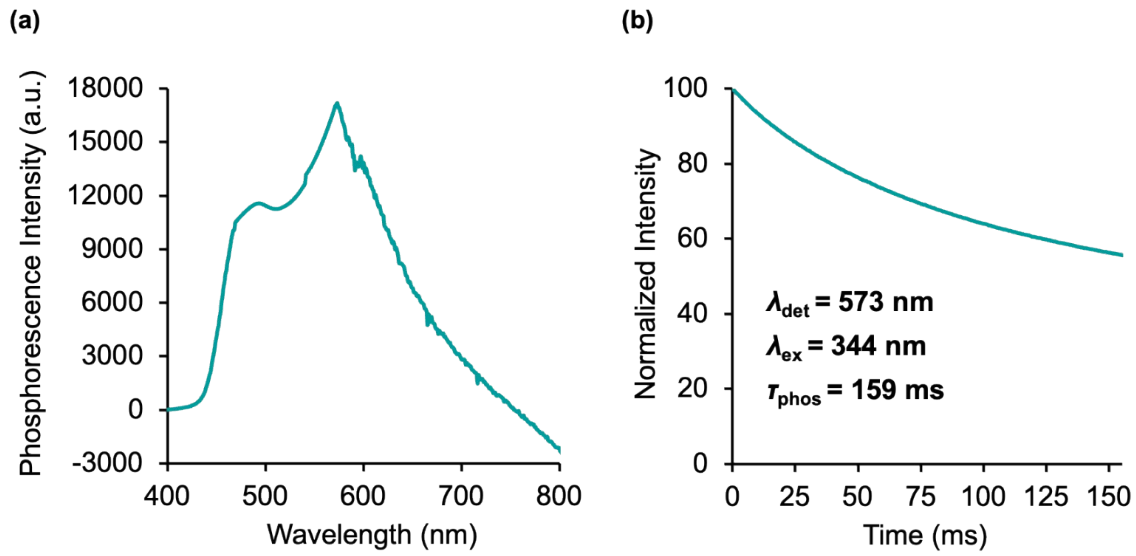

Fig. S31 (a) Steady-state phosphorescence spectrum (λ_{ex} = 344 nm) and (b) RTP lifetime decay curve (λ_{ex} = 344 nm and λ_{det} = 573 nm) of **B[6]**$_1$–**PFB[6]**$_1$ recorded at 77 K under nitrogen. The detection wavelength corresponds to the peak maximum in the steady-state phosphorescence spectrum recorded at 77 K under nitrogen.

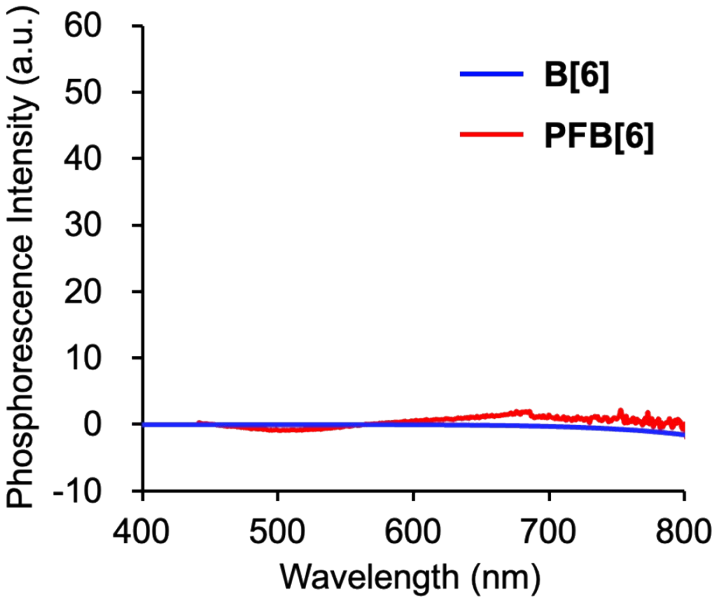

Fig. S32 Steady-state phosphorescence spectra of **B[6]** and **PFB[6]** (λ_{ex} = 290 nm for **B[6]**, λ_{ex} = 295 nm for **PFB[6]**). Both spectra were recorded at room temperature in air. The excitation wavelengths correspond to the peak maxima in the Kubelka–Munk transformed DR spectra of each compound (Fig. S29).

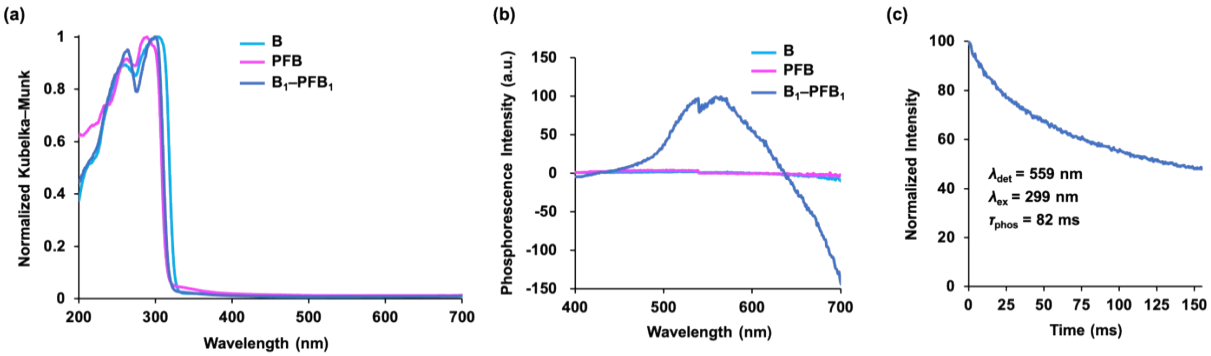

Fig. S33 (a) Kubelka–Munk transformed DR and (b) steady-state phosphorescence spectra of **B**, **PFB** and **B**$_1$–**PFB**$_1$ (λ_{ex} = 304 nm for **B**, λ_{ex} = 289 nm for **PFB** and λ_{ex} = 299 nm for **B**$_1$–**PFB**$_1$). (c) RTP lifetime decay curve of **B**$_1$–**PFB**$_1$. All spectra in (a), (b) and (c) were recorded at room temperature in air.

Table S1 Crystallographic data for **B[6]** with cyclohexane and **PFB[6]** with cyclohexane.

	B[6] with cyclohexane = **B[6]**•C_6H_{12} (CCDC-2531301)	**PFB[6]** with cyclohexane = **PFB[6]**•C_6H_{12} (CCDC-2531501)
Formula	$C_{144}H_{144}O_{12}$	$C_{132}H_{60}F_{60}O_{12}$
Formula weight	2066.58	2977.80
Temperature (K)	100	120
Crystal size (mm^3)	0.304 × 0.272 × 0.172	0.34 × 0.16 × 0.09
Crystal system	hexagonal	triclinic
Space group	*P*6*cc*	*P*-1
a (Å)	27.4224(6)	17.197(3)
b (Å)	27.4224(6)	18.846(4)
c (Å)	34.2315(13)	19.143(4)
α (deg)	90	76.90(3)
β (deg)	90	85.27(3)
γ (deg)	120	89.25(3)
V ($Å^3$)	22292.9(13)	6022(2)
Z	8	2
D_{calcd} (g cm^{-3})	1.231	1.642
Reflections collected	223587	67979
Independent reflections	13217 [R_{int} = 0.1376, R_{sigma} = 0.0757]	19697 [R_{int} = 0.0900, R_{sigma} = 0.0781]
2*θ* range for data collection (deg)	3.72–134.298	9.336–127.372
F_{000}	8832.0	2976.0
μ(Cu K*α*) (mm^{-1})	0.599	1.509
Limiting indices	$-32 \le h \le 32$ $-31 \le k \le 32$ $-40 \le l \le 40$	$-19 \le h \le 19$ $-19 \le k \le 21$ $-22 \le l \le 22$
Data/restraints/parameters	13217/1969/1620	19697/8319/2781
Goodness-of-fit on F^2	1.761	1.889
R_1 ($I>2\sigma(I)$)[a]	0.1245	0.1337
wR_2 ($I>2\sigma(I)$)[a]	0.2889	0.3303
R_1 (all data)[a]	0.1714	0.2423
wR_2 (all data)[a]	0.3235	0.3900

[a] $R_1 = \Sigma||F_o| - |F_c||/|F_o|$; $wR_2 = \{\Sigma w(F_o^2 - F_c^2)^2/\Sigma[w(F_o^2)^2]\}^{1/2}$.

References

S1 G. M. Sheldrick, *Acta Crystallogr., Sect. C: Struct. Chem.*, 2015, **71**, 3−8.

S2 Y. Ma, X. Chi, X. Yan, J. Liu, Y. Yao, W. Chen, F. Huang and J.-L. Hou, *Org. Lett.*, 2012, **14**, 1532–1535.

S3 T. Ogoshi, T. Aoki, K. Kitajima, S. Fujinami, T. Yamagishi and Y. Nakamoto, *J. Org. Chem.*, 2011, **76**, 328–331.

S4 D. Cao, Y. Kou, J. Liang, Z. Chen, L. Wang and H. Meier, *Angew. Chem. Int. Ed.*, 2009, **48**, 9721–9723.

S5 D. Pendin, R. Norante, A. D. Nadai, G. Gherardi, N. Vajente, E. Basso, N. Kaludercic, C. Mammucari, C. Paradisi, T. Pozzan and A. Mattarei, *Angew. Chem. Int. Ed.*, 2019*,* **58***,* 9917–9922.

S6 T. Ogoshi, Y. Hamada, R. Sueto, Y. Sakata, S. Akine, A. M. P. Moeljadi, H. Hirao, T. Kakuta, T. Yamagishi and M. Mizuno, *Chem. Eur. J.*, 2019, **25**, 2497–2502.

S7 T. Ogoshi, K. Maruyama, Y. Sakatsume, T. Kakuta, T. Yamagishi, T. Ichikawa and M. Mizuno, *J. Am. Chem. Soc.*, 2019, **141**, 785–789.

S8 T. Ogoshi, K. Saito, R. Sueto, R. Kojima, Y. Hamada, S. Akine, A. M. P. Moeljadi, H. Hirao, T. Kakuta and T. Yamagishi, *Angew. Chem. Int. Ed.*, 2018, **57**, 1592–1595.

S9 K. Onishi, S. Ohtani, K. Kato, S. Fa, Y. Sakata, S. Akine, M. Ogasawara, H. Asakawa, S. Nagano, Y. Takashima, M. Mizuno and T. Ogoshi, *Chem. Sci.*, 2022, **13**, 4082–4087.

S10 H. Nishihara, T. Hirota, K. Matsuura, M. Ohwada, N. Hoshino, T. Akutagawa, T. Higuchi, H. Jinnai, Y. Koseki, H. Kasai, Y. Matsuo, J. Maruyama, Y. Hayasaka, H. Konaka, Y. Yamada, S. Yamaguchi, K. Kamiya, T. Kamimura, H. Nobukuni and F. Tani, *Nat. Commun.*, 2017, **8**, 109.

S11 H. Zhu, J. Liu, Y. Wu, L. Wang, H. Zhang, Q. Li, H. Wang, H. Xing, J. L. Sessler, and F. Huang, *J. Am. Chem. Soc.*, 2023, **145**, 11130–11139.